International Conference on
Nucleon Structure
Stanford, California
June 24-27, 1963

INTERNATIONAL CONFERENCE ON NUCLEON STRUCTURE

Stanford 1963

CONF-122-22

High Energy Elastic Scattering of $\pi^{\pm}$, p, $\bar{p}$ and $K^{\pm}$ by Protons (and Regge Pole Predictions)

by S. J. Lindenbaum

Brookhaven National Laboratory

INTRODUCTION

It will be perhaps more efficient if we spend a few minutes at first defining the simple theoretical concepts used in interpretation of the experiments so that readers not expert in this field can still follow the arguments.

The elastic differential scattering of a particle α by another particle β when both are spinless can be completely described in terms of a function of the usual Lorentz invariants s (the square of the total cms energy) and t (the negative of the four momentum transfer squared) as illustrated by the following Feynmann scattering diagram.

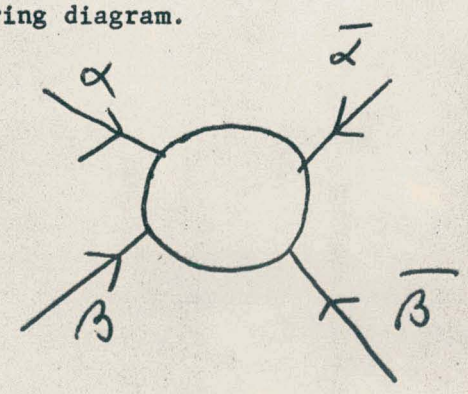

(1)

DISCLAIMER

where $s \equiv (P_\alpha + P_\beta)^2 = (E_\alpha{}^{cm} + E_\beta{}^{cm})^2 = m_\alpha{}^2 + m_\beta{}^2 + 2m_\beta\, E_\alpha{}^{lab}$ assuming β (2) at rest in Lab and $t \equiv (P_\alpha + P_{\bar{\alpha}})^2 = -2(P^{cm})^2 (1-\cos\theta^{cm}_{Scatt})$ where P is the (3) four momentum. The third usual invariant $u \equiv (P_\beta + P_{\bar{\alpha}})^2$ is determined by the (4) other two and any two of the three can be treated as independent variables and then can be used to determine the third. The invariant scattering amplitude can then be expressed by a complex function of s and t, namely A(s,t) so defined that: $d\sigma_{el/dt}(s,t) = 4\pi m_b{}^2/s^2 \left|A(s,t)\right|^2 = \left|A^1(s,t)\right|^2$ where $A(s,t) = A_r(s,t) + i\, A_i(s,t)$ (5)

Then the optical theorem states that:

$A_i(s,0) = s/8\pi m_b\, \sigma_t(s)$ and therefore (6)

$d\sigma_{el/dt}(s,0) \geq \frac{1}{16\pi}\left[\sigma_t(s)\right]^2 \; d\sigma(s,o)/dt_{opt}$ (7)

The L. H. S. of (7) becomes equal to the R. H. S. when $A_{re}(s,o) = 0$ and then $d\sigma_{el}(s,0)/dt = \frac{1}{16\pi}\left[\sigma_t(s)\right]^2 \equiv d\sigma(s,0)/dt_{opt}$. All evidence to date and the new data to be presented in this paper are consistent with $\left|A_i(s,0)\right|^2 \gg \left|A_{re}(s,0)\right|^2$ at high energies ($\gtrsim$ 10 Bev), $d\sigma/dt_{opt}$ has been well determined by the many total cross-section experiments[10,11,12].

The two most generally considered theoretical forms for A(s,t) have been based in earlier work on the optical model[1] and in the last two years on the Regge Pole Theory[2]. The simplest version of the optical model is the black absorbing disc or sphere and for this case:

$$d\sigma/d\Omega = \left|\frac{R.\ J_1(PR\sin\theta)}{\sin\theta}\right|^2$$

where R is the radius of the interaction. We now transform this into the Lorentz invariant form which for small angles becomes:

$$d\sigma/dt = \pi R^2 \left[\frac{J_1(R\sqrt{|t|})}{\sqrt{|t|}}\right]^2 \qquad (9)$$

For $R \approx 1$ fermi or less and $t \lesssim 0.3$ we can use the Gaussian approximation and we obtain:

$$d\sigma/dt \approx \pi R^4/4\; e^{-\left(\frac{R}{2}\right)^2 t} = d\sigma/dt_{opt}\; e^{-\frac{R}{2}^2 t} \qquad (10)$$

If we have a partially transparent but uniformly absorbing disc or sphere such that the fraction of the incident wave absorbed at the distance r, namely a (r) is within the nuclear radius a positive constant and no change of phase occurs, $a(r) = \bar{a}$ for $r \leq R$, $a(r) = 1$ for $r > R$. Then formulae (9) and (10) remain the same except the R. H. S. is multiplied by $(\bar{a})^2$.

Hence,

$$d\sigma/dt = \pi R^2 (\bar{a})^2 \left| \frac{J_1 (R\sqrt{|t|})}{\sqrt{|t|}} \right|^2 \approx d\sigma/dt_{opt}\, e^{-\frac{R^2}{2}t} \qquad (11)$$

For a Gaussian pure imaginary absorbing potential a similar form would correspond to the r.m.s. radius. Therefore, the R determined from eq. (11) is a relatively good way to phenomenollogically define the effective radius of the interaction from elastic scattering experiments. Once having defined a radius we can better define an effective opacity 0 in the following way:

$$0 = \frac{(\sigma t_{tot} - \sigma_{el})}{\pi R^2} = \frac{(\sigma \text{ inelastic})}{\pi R^2} \qquad (12)$$

(Since in this case, the definition of 0 does not depend on phase shift in the transmitted wave).

Until about two years ago it was generally believed that at incident energies ≥ 10 Bev, R in eq. (10) was not a function of s or that the s dependence was very weak and that for any incident particle $(d\sigma_{el}/dt)_{\alpha,\beta} \approx \phi_{\alpha,\beta}(t)$; $\sigma_{tot_{\alpha,\beta}} \approx$ constant. Then the relativistic Regge pole theory was developed by arbitrarily adopting the exact methods Regge introduced for describing non-relativistic Schrodinger equation potential scattering by poles moving in the complex J plane as a function of energy. Chew and Frautschi and others[2] then associated a Regge pole trajectory with all particles and dynamic resonances and developed a relativistic Regge pole theory using analytic continuation and generalized crossing symmetry. For a single Regge pole* at high enough s originally estimated to correspond to $\gtrsim$ 10 Bev/c incident particle momentum and low t they obtained the expression $d\sigma_{el}/dt = f(t)\left(\frac{s}{s_o}\right)^{2\alpha(t)-2}$ where

---

*Note no spin effects are included and separate non-spin flip and spin flip amplitudes are replaced by one spin averaged amplitude.

the original estimates of $\alpha(t) \approx 1-t(\text{Bev/c})^2$. This expression differs (13) from the usual perfurbation theory or dispersion theory pole forumula since the α which represents the spin of the exchanged particle is now a decreasing function of t rather than a constant.

As a result of the crossing symmetry the α corresponds to a pole in the t-channel, of energy + t, whereas in the physical scattering region s-channel, $t \leq o$. It is clear from the above equation that the highest lying trajectories (i.e., those with the largest values of α) will be most important. Due to the constancy of p + p total cross section above, 10 Bev/c and the slow s variations of other cross sections, the dominant pole must obviously have $\alpha(o) \approx 1$ and the vacuum pole or Pomeranchuk Pole was introduced and assumed to be dominant in all strong interactions at high enough energy (originally estimated to correspond to $\gtrsim$ 10 Bev/c, incident particle momentum) with the usual assumption of parallel Regge trajectories.

The next highest lying trajectories would obviously be the vector mesons ρ and ω. Fig. 1 shows the most important Regge trajectories for forward elastic scattering. The ρ and ω and a second vacuum trajectory P' (introduced by Ig[illegible]) were developed into a three-four pole model in which the vacuum pole predominated and all total cross-section data were explained reasonably well.

It was shown that for the three pole model (3)

$d\sigma/dt = F(s,t)\left(\frac{s}{so}\right)^{2\alpha(t)-2}$ where the $\alpha(t)$ defined by (14) is an (14) equivalent one pole α which for p + p interactions differs only slightly from the vacuum pole α and F(s,t) has on the average only a weak s dependence compared to the exponential term s dependence.*

The assumption of the dominance of the vacuum pole in all interactions at high enough energy led to the most striking prediction of the Regge pole theory that the average slope of the $d\sigma_{el}/dt$ curve should increase logarithmically with increasing s in all interactions and so at very high energy the effective inter-

---

* One should note that at or very near $\alpha(t) = 1$ the exponential term is or approaches unity and has no s dependence.

action radius would grow logarithmically while the transparency of the interacting region would increas in such a way that the total cross-section remained the same.

To date this predicted effect has been observed[4] and definitely established for p + p interactions[5] but has definitely been contradicted[5] for π^- + p and π^+ + p elastic scattering in the 7-20 Bev/c range, and neither the vacuum pole nor the three-pole model predictions[3] have been consistent with these new experiments[5].

An equivalent one-pole analysis (eqs. 13 and 14) is a convenient way to parametrically represent the s dependence of $d\sigma_{el}/dt(s,t)$ irregardless of the validity of the simple versions of Regge pole theory, and more complicated possibilities including spin effects, other poles, cuts, etc. can also be discussed conveniently in terms of the equivalent one-pole analysis.

Elastic Scattering Experiments

The Brookhaven Counter Hodoscope Experiments. These elastic scattering experiments by Foley, Lindenbaum, Love Ozaki, Russell and Yuan[5,6] used an experimental arrangement shown in Fig. 2. Some of the earlier results of the experiment have been published (5). From a momentum analyzed (±1.5%) AGS beam one of the six particles $\pi^\pm$, p, $\bar{p}$, $K^\pm$ of the incident momentum 7-20 Bev/c was selected by a gas Cerenkov counter telescope and allowed to scatter in a liquid hydrogen target. Both the forward scattered particle and proton recoil were detected by a crossed slab hodoscope scintillation counter system which defined 144 counter areas for the forward scattered particle and 484 counter areas for the recoil and covered $\sim$ 10% of the availabe solid angle in the t range of $\approx$ 0.2 to 1.0. Another magnetic spectrometer setup to be described later was also used to obtain data points at $t \lesssim 0.2$. The outputs from the hodoscope counters were fed to 96 fast discriminator gates which were opened simultaneously upon a suitably generated trigger signal indicating a particle had struck each hodoscope. The 96 bits of in-

formation specifying an event were then transferred through the gates and the input stages of a digital automatic data handler to its magnetic core memory which had sufficient memory for 32 events per AGS pulse (~ 1.5-3 sec period). Between AGS pulses these data bits were recorded on magnetic tape and simultaneously transmitted over telephone lines to the Brookhaven Merlin Computer for on-line immediate processing according to a previously debugged program.

At the end of each data-taking period, the computer determined the elastic scattering events by coplanarity and kinematic angle requirements and subtracted a background generally one to a few per cent for most of the t range but for a few cases at highest t values, it became as high as 30%. The computer then calculated for each of 12 t ranges, the absolute elastic cross-section, $d\sigma/_{dt}$ and its statistical error. Except for second order corrections, (such as accidentals, exact normalization) slight changes in beam momentum and angle measured more accurately during the data run, and other small corrections, experimental values were available anytime for inspection upon computer print out command, and also oscilloscope displays of the kinematic requirements and the associated elastic scattering peaks were continuously available in our data trailer on the AGS floor. Therefore, the restuls of the experiment were known as it was run. We were able to obtain at least 10,000-20,000 elastic scattering events/hour where beam rates were high and this represents more than one and perhaps two orders of magnitude increase over previous experiments and furthermore, our systematic errors were considerably smaller than for previous experiments. For further details of the apparatus see (5) and (7).

p + p and $\pi^{\pm}$ + p Elastic Scattering

Figs. (3) and (4) summarize the results obtained for 7-20 Bev/c p + p and π^+ + p and π^- + p elastic scattering. The graph ordinate is proportional to $d\sigma/dt \Big/ (d\sigma/dt)_{opt}$ with the normalization chosen for convenience so that the ordinate

equals $d\sigma/dt \left[\text{mb}/(\text{Bev}/c)^2\right]$ at 20 Bev/c. Corrections were made for beam contamination, background, accidentals, pion decay, etc. The errors shown are compounded estimates of relative errors which affect conclusions regarding shrinkage. These include statistical errors (standard deviation), relative efficiency errors, relative normalization errors, uncertainty in background subtraction, and relative errors introduced in calculating mean t values due to momentum and angle uncertainties.

The absolute normalization is estimated to be uncertain by 5% for p + p and about 7% for $\pi^{\pm}$ + p. We believe a 10% uncertainty in absolute scale is a sufficently conservative limit, with the relative scale factor between the two different types of incident particles uncertain to 5% or less.

The fits shown are of the form $d\sigma/dt = e^{a\ bt+ct^2}$ and the c co-efficient is always positive, gnerally $\approx$ 20% of the b co-efficient with an error < 1/4-1/2 the co-efficient for each individual momentum, and is clearly statistically significant. Therefore, slope analyses and optical theorem extrapolation analyses of data which do not include the ct^2 term are unrealistic. Brandt et al[8] have recently reported a bubble chamber experiment on 10 Bev/c π^- + p elastic scattering data, which within errors agrees with our 10 Bev/c data. Table I summarizes the parameters obtained for our $\pi^{\pm}$ + p data.

Regge Pole Analysis

In the p + p case (Fig. 3) one can observe a clear Regge type shrinkage with increasing s or incident momentum of the $d\sigma/dt \Big/ d\sigma/dt_{opt}$ fit curves, but in the π^+ + p case (Fig. 4) one fit $e^{a+bt+ct^2}$ independent of s (or incident momentum) represents the data well (χ^2 of 63 where 48 is expected for π^+ + p, χ^2 of 51 where 47 is expected for π^- + p). As can be seen in Fig. 1, the π^- + p and π^+ + p fits are within errors about the same at low t but there is a somewhat greater average slope in the π^- + p fit.

Both the one pole and three pole model (or multi-pole) model can be represented by an equation of the form:

$$\log \left(d\sigma/dt \Big/ d\sigma/dt_{opt} \right) = \log F(s,t) + [2\alpha(t)-2]\log s \qquad (15)$$

where $\alpha(t)$ is independent of the choice of s_o which is absorbed in $F(s,t)$, and the s dependence of F is absent in the one pole model and relatively weak in the three pole model. Therefore, neglecting s dependence of F(i.e., equivalent one pole analysis) the best way to determine $\alpha(t)$ at a particular t* for a set of data at different s is from eq. 15 where the slope of the linear least squares fit gives $2\alpha(t) - 2$. The results of such analyses are shown in Figs. (5), (6), and (7).

We then let $\alpha(t) = a + bt$**and found good fits to our data in all cases as follows:

$$\text{7-20 Bev/c } \alpha_{p+p}(t) = (1.07 \pm .03) + (0.83 \pm 0.07)t \qquad (16)$$

$$> \text{10 Bev/c - 20 Bev/c } \alpha_{p+p}(t) = (1.0 \pm 0.05) + (0.65 \pm 0.13)t \qquad (17)$$

$$\text{7-20 Bev/c } \sigma_{\pi^- + p} = (0.96 \pm 0.03) + (0.008 \pm 0.080)t \qquad (18)$$

$$\text{"} \qquad \sigma_{\pi^+ + p} = (0.96 \pm 0.04) + (0.086 \pm 0.097) \qquad (19)$$

considering P, P', ρ and ω poles with spin averaged amplitudes and parallel Regge trajectories we cannot explain the above results.

From the lack of any difference within statistical errors for $\alpha_{\pi^- + p}$ and $\alpha_{\pi^+ + p}$ and the lack of or very slow convergence of the small difference of total $\pi^- + p$ and $\pi^+ + p$ cross-section[10] and the small difference of total $(p + p)-(\eta + p)$ one can conclude that the ρ pole is relatively weakly coupled and neglect it***(3b).

The ω has wrong G parity (= -1) and does not enter in $\pi^{\pm} + p$ case. The remaining P and P' therefore both being vacuum poles would be expected to be coupled with the same positive sign in $\pi^+ + p$ and $\pi^- + p$. The relative amplitude of P' and P is fixed by total cross-section data.(10)

In the p + p case the P' and ω must have approximately equal and opposite imaginary amplitudes at t = o to give energy independence of σ_t (p + p) above 10 Bev/c and the magnitude of these amplitudes is estimable from the difference of $\sigma_t(\bar{p}+p)-\sigma_t(p+p)$ (11)

*Second order variations in t were interpolated out using the least squares fits to our data.

**a must not be assumed unity, since real amplitudes and changes in functional form near t = o, or normalization errors in total cross-section data will affect a.

***One should remember that we are talking about spin averaged amplitudes in regard to total cross-section experiments, since if one allows a vastly different non-flip and spin flip amplitude, the total cross-section experiments only measure the non-flip amplitude.

From the foregoing one would conclude that p + p and π^- + p and π^+ + p all would exhibit comparable shrinkage describable by a similar $\alpha(t)$, which is obviously contradicted by the experiments and the Regge pole hypothesis made above are incorrect.

The effects of more complex assumptions (separate and arbitrarily coupled spin flip amplitudes, cuts, more poles, etc.) can be more fruitfully discussed later.

K^+ + p Elastic Scattering

Fig. 8 presents our elastic scattering data for K^+ + p at incident momenta 7-15 Bev/c. The data was treated in a similar fashion as for $\pi^\pm$ + p. Since from the total cross-section data (12) it was concluded there is no momentum dependence in this momentum interval $d\sigma/dt$ mb/(Bev/c)^2 was plotted directly as the ordinate without the previously used normalization. The least squares fits shown are of the previously used form $d\sigma/dt = e^{a+bt+ct^2}$.

The results of the equivalent one pole analysis for $\alpha(t)$ are shown in Fig. 9.

The least squres linear fit for $\alpha(t) = a + bt$ gave the result.

$$\alpha(t) = (0.71 \pm 0.20) + (0.003 \pm 0.230)t \qquad (20)$$

The error on a allows for $\approx$ 5% estimated uncertainty in the flatness of the K^+ + p total cross-section and other systematic errors. The difference of a form unity is not considered significant.

The real test of Regge type shrinkage is the b co-efficient in $\alpha(t) = a + bt$. This is so because any real amplitude varying with incident momentum or relative normalization error in either the incident momentum dependence of the total cross-section or the $d\sigma_{el/dt}$ will sensitively change a form unity. However b will be almost independent of any normalization effect or change in real amplitude with incidient moemntum* since it measures the change in shape of the differential elastic

*Provided there is no coupled s and t dependence.

scattering curve as a function of s rather than the change in normalization and it is therefore essentially only the bt terms in $\alpha(t)$ which gives the Regge shrinkage effects. We see from eq. (19) that b is consistent with zero (i.e., no shrinkage). The systematic part of the error in b can be well estimated to be a negligible fraction of the error since the same apparatus and calibrations were used as in the very accurate p + p and $\pi^{\pm}$ + p experiments. Therefore, statistical probability considerations can be directly applied to this error, and we see that ≈ 3.7 standard deviations are required to obtain the same value of b as for p + p and only ≈ 1.8 deviations to obtain $\approx \frac{1}{2}$ the value of b as for p + p. Naturally negative values (anti-shrinkage) of b are just as likely as positive values since the mean value is near zero.

From the Regge pole theory point of view the K^+ + p shrinkage behavior was expected to be similar to p + p since the same Regge poles enter and the flatness of the K^+ + p total cross-section implied the same cancellation of ω and P' poles which was used in the p + p case, and the behavior of the K^- + p cross-section also supports this.

Another interesting point is that in the fits $d\sigma/dt = e^{a}e^{(b+ct)t}$ to the data the average value of $\overline{b + ct}$ is comparable for positive and negative pions and protons over the 7-15 Bev/c incident momentum range, whereas for the K^+ + p the $\overline{b + ct}$ is considerably less (by about $\sim 30\%$) implying that the K^+ is a small particle. The question of effective particle radii will be treated in more detail later.

$\bar{p}$ + p Elastic Scattering

Fig. 10 presents our data for $d\sigma_{el}/dt$ for p + p at 7.2, 9.0 and 11.9 Bev/c incident momenta[6]. The ordinate is $d\sigma/dt \; \frac{d\sigma}{dt}_{opt} \; \frac{mb}{(Bev/c)^2}$ with the normalization chosen so that the ordinate is equal to $d\sigma/dt$ $(mb/(Bev/c)^2$ at the highest incident momentum 11.9 Bev/c.

The average slope of the exponential fit is considerably steeper than for all other interactions measured.

Fig. 11 shows an equivalent one Regge pole analysis. The result is $\alpha_{\bar{p}+p}(t) = (0.79 \pm 0.36) - (1.39 \pm 1.36)t$ and due to the size of the error is clearly inconclusive.

$K^- + p$ Elastic Scattering

Fig. 12 presents our data[6] for $d\sigma_{el}/_{dt}$ $(K^- + p)$ at incident momenta of 7.2 and 8.9 Bev/c.

The average slope is comparable with that for pions and protons, and considerably larger than for K^+ (see sect. on Particle Radii).

Effective Particle Radii

In the Introduction we saw that for $t \lesssim .3$ and $R \approx 1$ fermi.

The black disc or sphere or constant absorption disc optical model elastic scattering can be presented by $d\sigma/dt = d\sigma/dt_{opt}\, e^{-\left(\frac{R}{2}\right)^2 t}$ and that an exponential form would also correspond to a Gaussian potential. Hence R is a reasonable definition of an effective radius for the interaction. Unfortunately, our data exhibit significant c co-efficients* when we let $d\sigma/_{dt} = e^{a+bt+ct^2}$ and therefore $R = \phi(t)$ so that an effective radius should be defined as the slope of the exponential at a particular value t, $R = b + 2ct$ which is expected to reflect the average or effective behavior of the radius and, of course, this t value should be in the measured range.

We believe that $t \approx 0.1$ to 0.2 corresponding to transverse momental of $\approx$ 300-450 Mev/c (and distance $\approx$ 2/3 to 1/2 fermi) is a reasonable compromise in averaging over outer pion cloud and core regions of the interactions, and we use $t \approx 0.2$ since in all cases, our data extends down to that region. Since a proton target is common in all cases, we may for convenience, associate the radius of the interaction with the incident particle.

---

*of a magnitude outside error in linear approximation for Gaussian potential

Fig. 13 shows our p + p results for the exponential slope = $(b + 2ct) \rightarrow b + 0.4\ c = \left(\frac{R}{2}\right)^2$ at $t = 0.2$. Errors include statistics and estimates of systematic errors in the estimates. The lower energy data, including estimates of the error in making comparison from linear fit (no ct' beam) is also shown. (21)

The slope of the exponential at $t \approx .2$ will be expected to only loosely reflect the Regge pole shrinkage effects with large errors since the conclusions on Regge pole effects are based on all the data, not just at one t value. We find a trend for a growth of effective radius with increasing momentum as we would expect with relative values changing from 1.06 ± 0.04 f (at 7 Bev/c) to $\approx 1.18 \pm 0.05$f. The average effective radius $\approx 1.14 \pm 0.015$f (7-20 Bev/c). A similar plot for effective radii in π^- + p and π^+ + p is given in Fig. 14.

Here we see no trend for change with incident momentum. The average effecitve radii for (7-17 Bev/c) π^- + p $\approx 1.11 \pm 0.018$f

" π^+ + p $\approx 1.05 \pm 0.022$f

The difference in effective radii for π^+ + p and π^- + p is not considered necessarily signficiant. As one can also note on the average (from 7-20 Bev/c) pions* and protons have almost comparable radii.

Fig. 15 shows the effective radii deduced for K^+ + p, K^- + p and $\bar{p}$ + p interactions.

It is clear that $\bar{p}$ + p effective radius is much larger than observed for pions and protons. For 7-12 Bev/c the average eff, rad ($\bar{p}$ + p) = 1.35 ± 0.08f and may be increasing at lower momenta.

The K^- + p (7-9 Bev/c) on the other hand, has $R_{eff} = 1.13 \pm .04$ and is comparable with protons and pions* in size. The average K^+ + p eff, radius for 7-15 Bev/c is 0.95 ± .04 and considerably smaller than the K^- or π^+, π^- or proton effective radii.

---

* At least for negative pions, since π^+ + p may have a somewhat smaller effective radius.

Hence to summarize the effective particle size, the $\bar{p}$ appears to be effectively largest, then π^-, π^+, K^- and p (on average neglecting Regge effects) are all comparable, followed by the K^+ which is the smallest.

Magnetic Spectrometer Setup for low t Data

The previously described hodoscope equipment (co-incidence setup) selected elastic scattering events by kinematic requirements (coplanarity and kinematic angle) over the t range $\approx$ 0.2 to 1.0(Bev/c)^2. For the lower t points we used magnetic spectrometer setup shown in Fig. 16. This was necessary since the recoil protons stopped in the target at low t.

Hodoscopes H_1 and H_2 consisting of 28 and 80 respectively vertical slab counters 6" x ¼" wide measured the angle by which the incident particle was scattered by the Hydrogen target in the horizontal plane with a resolution of ± 1 mrad.

Hodoscope H_3 consists of crossed slab counters 2.5 inches wide by 30 inches long arranged in an array of 120" wide by 30" high measured both the vertical and horizontal position of the scattered particle after passing throug the analyzing magnets. The momentum of the scattered particle was measured with a resolution of ± 1.5%. The triggering logic was arranged so that a particle was required to scatter by 15-55 mrad, strike H_3 and to have a momentum (>15-50% P incident) depending upon the scattering angle to open the gates from the counters. Coding was used to reduce the number of input pulses to 96 and the previously described data handling system and on line computer was used.

For those events having only one particle per hodoscope the space angle and momentum of the scattered particle was calculated. The momentum spectrum of the particles within each angular bin$^{(5\ mrad)}$ was calculated and generally showed a peak at the proper elastic momentum $\approx$ 5-10 times background.

The on line computer totaled the number of possible elastic particles at the right momentum in each bin, calculated and subtracted the background, calculated absolute cross-sections $d\sigma/_{dt}$, its statistical error and the mean t values for the bin. Final 2nd order corrections to the data,as previously,were made after the experiment.

Hodoscopes H_1 and H_2 measured incidnet beam direction to < 0.2 mrad. The analyzing magnets were used to set and measure beam momentum to < 0.2%, using 3 centering counters near H_3. So far we have evaluated the data from this setup only for p + p and π^- + p. Typical results at 2 momenta of the magnetic setup and compared to the previous results (co-incidence setup) are shown in Fig. 17 (P + p) and in Fig. 18 (π^- + p). A single calculated relative normalization factor well within the relative normalization errors of the two setups was used. There is considerable overlap of the two types of data especially at the higher momenta and the agreement between these two systematically entirely different methods is very good. Fits of the form $d\sigma/_{dt} = e^{a+bt+ct^2}$ are shown to all the data combined at the two momenta and an intermediate one.

The three p + p fits show the well-defined Regge shrinkage increasing with increasing t , whereas the π^- + p fits show no such effect. The random wandering of the π^- + p fits at high t just reflects the poorer statistics in this region. These and similar fits to all π^- + p and p + p data will be used later to estimate the total elasticcross-sections and $d\sigma/_{dt}$ at t = o. We expect in the near future to complete the treatment of the low t (magnetic setup) data for π^+, $K^\pm$, and $\bar{p}$ incident particles.

Total Elastic Cross-sections

Having fits to the data of the form $d\sigma/_{dt} = e^{a+bt+ct^2}$, it is an easy matter to assume this functional form and integrate* and obtain the total cross-section. Naturally, both the overall accuracy of the result and the size of possible

*The integration was carried to t = 1 (Bev/c)^2. The error in neglecting higher t contributions is estimated to be entirely negligible.

extrapolation errors are reduced by very low t points and therefore the data obtained by the magnetic spectrometer method is particularly valuable in this respect. So far we have evaluated all the data including the magnetic spectrometer setup for the $\pi^- + p$ and $p + p$ so we will treat this data first.

Fig. 20 (a) shows the total elastic cross-sections we obtained from $p + p$ and $\pi^- + p$ data. All sources of relative error have been included in the error points but the absolute scale factor is, of course, uncertain by the same constant (5-10%) as for the difference of the cross-sections.

Results from other experiments in this momentum region are also shown and it is clear there is a good agreement within errors. There is a systematic trend in our $p + p$ data for a decrease of the elastic cross-section with increasing momentum, but this effect is either small or absent in our $\pi^- + p$ data.

Fig. 19 shows σ_{el}/σ_{tot} for our $p + p$ and $\pi^- + p$ data and is substantially larger for $p + p$, implying the pion is more transparent.

Although σ_{el} $(\pi^+ + p)$ is not shown, it is estimated from our co-incidence setup data ($t \approx 0.2$ - 1.0) that the cross-sections are similar to those for $\pi^- + p$ but perhaps $\sim$ 7% lower in value.

The elastic cross-sections for $\bar{p} + p$, $K^+ + p$ and $K^- + p$ are obtained from an integration of the co-incidence setup data only and are shown in Fig. 20(b).

The forthcoming final anlaysis of the magnetic spectrometer data for these particles will provide better final values.

Optical Theorem

The optical theorem prediction in convenient practical units can be expressed as $\left(d\sigma/dt \text{ mb}/(\text{Bev/c})^2\right)_{t=0} \geq 0.051(\sigma_{tot})^2 (\text{mb})^2$ where the equality applies for no real part of the scattering amplitude.

Fig. 21 is a plot of a comparison of the extrapolation of our data (magnetic and co-incidence) and the optical theorem prediction by using the fits $d\sigma/dt = e^{a+bt+ct^2}$

and setting t = o. We have used our previous normalization method so that we plot an ordinate $\propto d\sigma/dt \Big/ \frac{d\sigma}{dt}_{opt}$ and the normalization is such that the ordinate is $d\sigma/dt \left(mb/(Bev/c)^2\right)$ at 20 Bev/c.

The dotted straight line then represents the optical theorem prediction.

The errors shown are relative errors only, and, of course, the same absolute scale uncertainty (5-10%) exists as for the differential cross-section data.

The π^- + p data agree well with the optical theorem and show no significant variation with incident momentum.

The p + p data, on the other hand, although they agree well with the optical limit in the region of 17-20 Bev/c show a systematic tendency to be above at lower momenta. Considering the absolute scale uncertainty, and the size of the relative errors, and possible relative errors as a function of momentum in the p + p and π^- + p total cross-section, we do not believe that the precision of the present analysis allows one to definitely conclude that there is convincing evidence for a real amplitude in the p + p case, when one considers all the possible systematic errors. However, we shall further investigate this point*. From an extrapolation of the π^+ + p co-incidence data we expect a similar result as for π^- + p, namely consistency with the optical theorem. However, for a critical evaluation of π^+ + p, K^+ + p, π^- + p and p + p in regard to the optical theorem we must await the completion of the magnetic data analysis.

Opacity

Our data for the p + p case yields the following approximate estimate for the average opacity using eq. (12)

$\bar{0} \approx 0.74 \pm 0.022$ and

For both positive and negative pions the average opacity is consistent with $\bar{1}.5 \pm 0.03$

---

*Note added after Conference--See paper by Gottfried which reports observation of an interference effect between the coulamb amplitude and a real part of the p + p scattering amplitude for 6.5 and 10.5 Gev/c p + p interaction.

For positive Kaons (7-15 Bev/c) $\bar{0} \approx 0.55 \pm 0.04$

For negative Kaons (7-9 Bev/c) $\bar{0} \approx 0.51 \pm 0.04$

For anti-protons (7-12 Bev/c) $\bar{0} \approx 0.83 \pm 0.07$

At 3.25 Bev/c $\bar{0} \approx 0.96 \pm 0.05$. (15a)

Discussion

With the advent of the Regge pole theory it was the great hope of many that finally a simple and definite prescription for two body final states at high-enough energy had been found.

It was originally generally considered that perhaps in the neighborhood of $\gtrsim$ 10 Bev/c the vacuum pole would dominate sufficiently so that effects of other poles might be neglected. The total cross-section data (10-12) and other reasons then made it clear that other poles, including the next highestlying trajectories, the ρ and ω vector mesons should be included and a second (Igi's) vacuum pole P' or equivantly a distorted ABC trajectory. This led to the four-pole model which immediately became the three-pole model as the ρ coupling appeared to be relatively weak. Spin-averaged amplitudes and parallel and approximately straight line Regge pole trajectories were assumed of average slope deduced from the nucleon trajectory.

The three-pole model or even the vacuum pole model alone can be easily made to fit all total cross-section data and the results of our p + p (7-20 Bev/c) elastic scattering experiments which exhibited Regge shrinkage compatable with the original estimate, and for which we determined from an equivalent one-pole analysis that

$$\alpha_{p+p} = (1.07 \pm .03) + (0.83 \pm 0.07)t$$

But then we cannot avoid a prediction for substantial Regge shrinkage for our (7-17 Bev/c) $\pi^+ + p$ and $\pi^- + p$ which is completely incompatable with our high precision results for no Regge shrinkage within small errors.

$$\alpha_{\pi^- + p} = (0.96 \pm 0.03) + (0.008 \pm 0.080)t$$

$$\alpha_{\pi^+ + p} = (0.96 \pm 0.04) + (0.086 \pm 0.097)t$$

Therefore, we must introduce additional effects. The ρ pole is shown to have a small effect since the $\alpha(t)$ is the smae within errors for $\pi^+ + p$ and $\pi^- + p$ and the scattering amplitudes have it coupled equally and oppositely in the two cases.

The $K^+ + p$ ealstic scattering would be expected to exhibit similar shrinkage behavior to the p + p since the same Regge poles are involved and P' and ω are also coupled oppositely (imaginary amplitudes) to obtain the constant total cross-section just as in the p + p case. However, we find the $K^+ + p$ consistent with no Regge shrinkage within errors and it will take ≈ 3.7 standard deviations to obtain the same slope for the equivalent vacuum pole trajectory as in the p + p case.

If we allow enough new arbitrary parameters we should eventually, of course, succeed in explaining any finite set of experimental data, but such explanations may well be just convenient parameterizations.

One way to obtain more parameters and possibly explain these results is to allow separate spin flip and non-flip co-effeicients with arbitrary couplings for the four poles we have already considered.*

Another way is to admit cuts in addition to Regge poles as Mandelstam and Amati etal have shown their effects to be substantial (17).

Gatland and Moffat (18) have arbitrarily assumed the energy variable s enters the equations in the normalized form only $= \frac{s}{2m_\alpha m_\beta}$ and then tried to explain our experimental results in terms of a single vacuum pole and a fixed cut. This makes $W_{\pi^{\pm} p} \gtrsim 6.5 \left(W_{p + p}\right)$ and allows the cut to dominate $\pi + p$ (which are more asymptotic), giving little shrinkage while the vacuum pole dominates p + p.

Also according to these authors with a scheme of this type, the $K^+ + p$ should show very little shrinkage effect.

Of interest is a recent conclusion by Freund and Oehme[19] that it is possible but not easy to obtain a non=shrinking diffraction pattern within the framework of causal dispersion theory.

Let us now summarize some of the other general features of the elastic scattering interactions we have observed.

---

*Critical tests of such an approach are being considered by G. Chew and collaborators, Private Communication.

The effective radii [see def eq. (9)] of $\pi^+ + p$ and $\pi^- + p$ interactions exhibit no momentum dependence (from 7-17 Bev/c) and have an average value of 1.08 ± 0.015 which agrees within errors with the average value of lower momentum data. The p + p interaction eff radii exhibit in general an expansion with increasing momentum (reflecting the Regge shrinkage effect), changing from $\approx 1.06 \pm 0.04$f at 7 Bev/c to $\approx (1.18 \pm 0.05)$f at 20 Bev/c. The (7-20 Bev/c) p + p average effective radius is $\approx 1.11 \pm 0.02$f. Hence, close to the average pion radius.

The average $K^+ + p$ radius (7-15 Bev/c) is 0.95 ± 0.04 and is significantly lower than for the incident pions and the protons. However, the (7-9 Bev/c) $K^- + p$ average eff radius 1.13 ± 0.04 is comparable to that for incident pions and protons.

The average $\bar{p} + p$ radius (7-12 Bev/c) is 1.35 ± 0.08 and is significantly larger than for the incident pions and protons and is probably increasing with lower momenta ($\sim$ 3.25 Bev/c).

One cannot, unfortunately, easily directly relate these nuclear interaction radii with the electromagnetic radii determined by the classic experiments started many years ago by Hofstadter and co-workers at Stanford[20]. This is so because the electromagnetic interaction radius is more sensitive to the spatial distribution of charge but the nuclear interaction radii are mostly determined by the radius out to which the particular nuclear interaction is resonably strong.

As far as opacity is concerned, the $\bar{p} + p$ is most opaque (7-17 Bev/c) $\bar{0} \approx 0.83 \pm 0.07$ increasing to $\bar{0} \approx 0.96 \pm 0.05$ at 3/25 Bev/c (7-20 Bev/c).

Next comes p + p (7-20 Bev/c) with $\bar{0} = 0.74 \pm 0.022$ and finally, the mesons, pions (7-17 Bev/c) and Kaons (7-15 Bev/c) all seem to have an opacity consistent with $\bar{0} \approx 0.55 \pm 0.04$.

The extrapolation of $d\sigma/dt$ to $t = o$ and comparison with the optical theorem gives good agreement within errors for 7-17 Bev/c $\pi^- + p$ but in the case of (7-20 Bev/c) p + p there is a considerable systematic tendency for higher values ($\sim$ 10%) than predicted below 15 Bev/c. However, we do not conclude this effect is significant since we cannot rule out that possible systematic errors in all the relevant

quantities, including total cross-sections, would not reduce this effect to an inconclusive one. However, we are analyzing this problem further.

Various total elastic cross-sections are plotted in Figs. 20(a) and (b).

Finally, I would comment that when reviewing all of the elastic scattering data, we have just considered in the 7-20 Bev/c region, and total cross-section measurements, I am more impressed with the many differences observed than the few similarities and it, therefore, appears that the explanation of these phenomena may be quite complex, and its uniqueness quite uncertain.

REFERENCES

(1) (a) Fernbach, S., Serber, R., Taylor, Phys. Rev. 75, 1382 (1949)

(b) Mathews and Salan, Nuovo cimento XXX1, 2694 (1961)

(c) Serber, R., Phys. Rev. Letters, 10, 357 (1963)

(2) (a) Chew, G. F., Frautschi, S. C., Phys. Rev. Letters, 1, 394 (1961)

(b) Frautschi, S. C., Gell-Mann, M., and Zachariasen, F., Phys. Rev. 126, 2204 (1962), Chew, G. F., Frautschi, S. C. and Mandelstam, S., Phys. Rev. 126, 1202 (1962), Blankenbecler, R. and Goldberger, M. L., Phys. Rev. 126, 766 (1962), Udgaonkar, Phys. Rev. Letters 8, 142 (1962)

(3) (a) F. Hadjioannous, R. J. N. Phillips and W. Rarita, Phys. Rev. Letters 9, 186 (1962)

(b) S. D. Drell in Proceedings of International Conference on High Energy Physics, Geneva, 1962, p.897

(4) Diddens, A., Lillithum, E., Manning, G., Taylor, A., Waltar, T., and Wetherell, M., Phys. Rev. Letter 9, 108 (1962)

(5) K. J. Foley, S. J. Lindenbaum, W. A. Love, S. Ozaki, J. J. Russell and L. C. L Yuan, Phys. Rev. Letters 10, 376 (1963) and 10, 543 (1963)

(6) Unpublished Experiments by Foley, Lindenbaum, Love, Ozaki, Russell and Yuan. Also referred to as this experiment, in graph titles or our results in text.

References (cont'd.)

(7) Lindenbaum, S. J., Nuclear Instruments and Methods. "A Counter Hodoscope System with Digital Data Handler and On-line Computer for Elastic Scattering and Other Experiments at Brookhaven AGS", Instrumentation for High Energy Physics, Proceedings 1962 Conferences, page 297, North Holland Publishing Co., Amsterdam;Nuclear Instruments and Methods 20(1963)297-302;North-Holland Publishing Co.

(8) Brandt et al, Phys. Rev. Letters 10, 413 (1963)

(9) Baker, Jenkins, Read, Coconni, Coconni and Orear, Phys. Rev. Letters 9, 221 (1962)

(10) (a) Lindenbaum, Love, Niederer, Ozaki, Russell and Yuan, Phys. Rev. Letters 7, 352 (1961)

(b) G. vonDardel et al, Phys. Rev. Letters 8, 173 (1962)

(11) Lindenbaum, Love, Niederer, Ozaki, Russell and Yuan, Phys. Rev. Letters 9, 185 (1961)

(12) Baker, Cool, Jenkins, Kycia, Phillips and Read, Phys. Rev. 129, 2285 (1963)

(13) Fujii et al, Phys. Rev. 128, 1836 (1962)

(14) Ting, Jones and Perl, Phys. Rev. Letters 9, (1962)

(15)(a) Baltay et al (p.233) and Ferbel et al (p.70), Proceedings of 1962 International Conference on High Energy Physics at CERN

(b) Escoubes et al (Submitted to Physics Letters)

References (cont'd.)

(16) Bull and Garbutt, Phys. Rev. 130, 1182 (1962)

(17) Mandelstam--1962 Stanford Conference.
Amati, Fabini, Stangbellini and Tonin, Nuovo cimento 22, 569 (1961)

(18) Gatland and Moffat--submitted to Phys. Rev.

(19) Freund and Oehme, Phys. Rev. Letters 10, 450 (1962)

(20)(a) R. Hofstadter, Nuclear and Nucleon Scattering of High Energy Electrons, Annual Review of Nuclear Science 7, 231-310

(b) Aitken, Hofstadter, Hughes, Tannger and Yeaman, 1962 CERN Proceedings

TABLE I

Least squares fits of $\pi^{\pm}$ + p data in coincidence set-up $t \approx 0.2$ to 1 using the parametric form $\frac{d\sigma}{dt}\left[\frac{mb}{(Bev/c)^2}\right] = \left[\frac{\sigma_t\ (20\ Bev/c)}{\sigma_t\ (P)}\right]^2 e^{a+bt+ct^2}$ where t is in $(Bev/c)^2$. The error of a point in the calculated fit is less than the error obtained by treating parameters as independent due to the usual coupling of errors through the error matrix which reduces the independently calculated error by a factor of 2 to several in the middle of the data t range.

π^+ + p case

Incident Momentum Bev/c	a	Δa	b	Δb	c	Δc
16.67	3.30	0.175	+8.17	0.77	2.10	0.76
14.72	3.23	0.137	+7.56	0.66	0.96	0.69
12.71	3.38	0.119	+8.30	0.56	1.86	0.57
10.75	3.24	0.124	+7.37	0.61	0.83	0.65
8.76	3.41	0.114	+8.22	0.557	1.91	0.60
6.78	3.37	0.092	+7.94	0.45	1.73	0.46

π^- + p case

Incident Momentum Bev/c	a	Δa	b	Δb	c	Δc
16.92	3.33	0.167	+8.05	0.83	1.04	0.93
14.97	3.49	0.106	+9.17	0.50	2.65	0.51
12.96	3.43	0.096	+8.75	0.47	2.17	0.51
10.89	3.43	0.097	+8.47	0.48	1.63	0.51
8.86	3.54	0.088	+9.03	0.44	2.36	0.47
7.09	3.49	0.090	+8.82	0.44	2.19	0.47

π^+ + p case

All data taken together in one fit
χ^2 = 63 where 48 is expected

a	Δa	b	Δb	c	Δc
3.36	0.048	+8.10	0.23	1.75	0.25

π^- + p case

All data taken together in one fit
χ^2 = 51 where 47 is expected

a	Δa	b	Δb	c	Δc
3.48	0.041	+8.88	0.20	2.22	0.21

FIGURE CAPTIONS

Fig. 1. Chew-Frautschi Plot

Fig. 2 The Experimental Arrangement (5,6). A Counter Hodoscope (co-incidence set up) with Automatic Data Handling and on-line computer. Elastic Scattering is selected by coplanarity and kinematic angle requirements.

Fig. 3 $\frac{d\sigma}{dt}\left[\frac{\sigma_t(p)}{\sigma_t(20\ \text{Bev/c})}\right]^2$ in $\frac{\text{mb}}{(\text{Bev/c})^2}$ for (7-20 Bev/c) p + p Elastic Scattering which is proportional to $d\sigma/dt \Big/ \frac{d\sigma}{dt}_{opt}$ plotted versus t

Fig. 4 $\left[\frac{\sigma_t(20\ \text{Bev/c})}{\sigma_t\ (P)}\right]^2 \frac{d\sigma}{dt}\frac{\text{mb}}{(\text{Bev/c})^2}$ for 7-17 Bev/c π^+ + p which is proportional to $d\sigma/dt \Big/ \frac{d\sigma}{dt}_{opt}$ plotted versus t
The solid line is a least squares fit to all the π^+ + p data.
The dotted line is a least squres fit to all the previously reported π^- + p data.

Fig. 5a $\alpha(t)$ versus t, the black circles are 7-17 Bev/c (π^- + p). The open circles are 7-20 Bev/c p + p data and the solid triangles for p + p data above 10 Bev/c. (5)

Fig. 5b Compares $\alpha(t)$ from above 10 Bev/c data only for p + p and π^- + p (5,6)

Fig. 6 $\alpha(t)$ versus t for π^+ + p data (7-17 Bev/c)

Fig. 7 A compilation of $\alpha(t)$ for above 10 Bev/c p + p elastic scattering from (5,6) and the higher t points (4,9)

Figure Captions (cont'd.)

Fig. 8 $K^+ + p$ Elastic Scattering - This Experiment (6).

Fig. 9 $\alpha(t)$ versus t for $K^+ + p$: This Experiment (6).

Fig. 10 $\bar{p} + p$ Elastic Scattering: This Experiment (6).

Fig. 11 $\alpha(t)$ versus t for $\bar{p} + p$: This Experiment (6).

Fig. 12 $K^- + p$ Elastic Scattering: This Experiment (6).

Fig. 13 p + p effective radius in fermi (right hand scale) using definition in text (see eq. 21): This Experiment (6) and also (13).

Fig. 14 $\pi^{\pm} + p$ effective Radii: This Experiment: (6) and (8, 14).

Fig. 15 $K^+ + p$, $K^- + p$, and $\bar{p} + p$ effective Radii: This Experiment (6) and (15a, 15b).

Fig. 16 Magnetic Spectrometer set-up for This Experiment (6) which obtained data points in the range 0.02 to 0.6 depending upon momentum.

Fig. 17 p + p Elastic Scattering data at two typical incident momenta (8.88 and 19.58 Bev) with both magnetic and co-incidence set-up data shown. The fits are of the form $d\sigma/_{dt} = e^{a+bt+ct^2}$ and a third intermediate momentum fit is shown.

Figure Captions (cont'd.)

Fig. 18 π^- + p elastic scattering data at two typical incident momenta. The fits are of the form $d\sigma/_{dt} = e^{a+bt+ct^2}$ and a third intermediate momentum fit is shown.

Fig. 19 The ratio of the elastic to the total cross-section for p + p and π^- + p: This Experiment (6).

Fig. 20a The total elastic p + p and π^- + p cross-sections.

Fig. 20b The total elastic cross-section for $\bar{p}$ + p, K^+ + p and K^- + p: This Experiment (6) and(15a).

Fig. 21 Comparison of this experiment (6) with optical theorem (please note discussion in text).

CHEW AND FRAUTSCHI PLOT

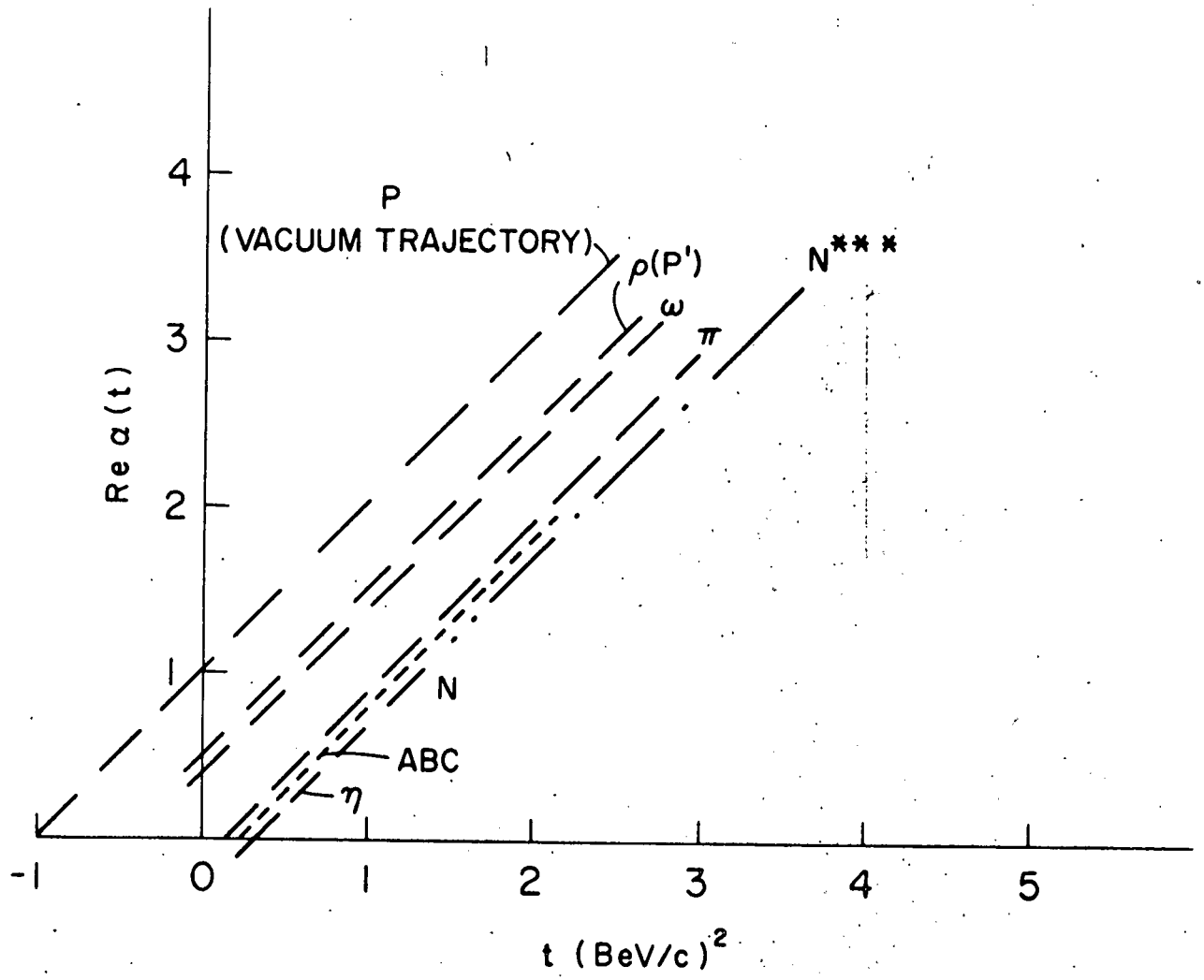

FIGURE 1

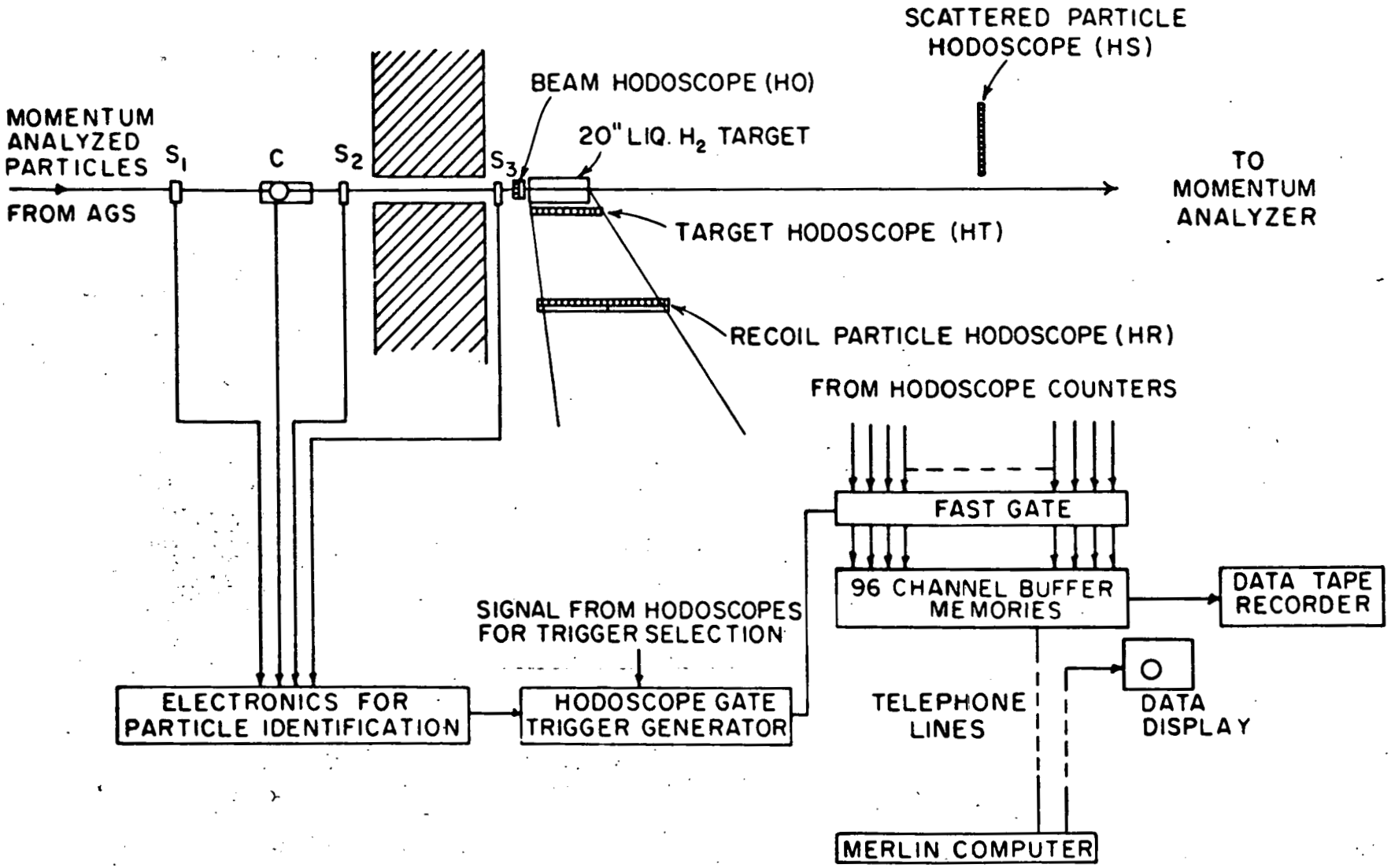
SCATTERED PARTICLE
HODOSCOPE (HS)
BEAM HODOSCOPE (HO)
20" LIQ. H_2 TARGET
MOMENTUM
ANALYZED
PARTICLES
FROM AGS
S_1
C
S_2
S_3
TO
MOMENTUM
ANALYZER
TARGET HODOSCOPE (HT)
RECOIL PARTICLE HODOSCOPE (HR)
FROM HODOSCOPE COUNTERS
FAST GATE
96 CHANNEL BUFFER
MEMORIES
DATA TAPE
RECORDER
SIGNAL FROM HODOSCOPES
FOR TRIGGER SELECTION
ELECTRONICS FOR
PARTICLE IDENTIFICATION
HODOSCOPE GATE
TRIGGER GENERATOR
TELEPHONE
LINES
DATA
DISPLAY
MERLIN COMPUTER

FIGURE 2

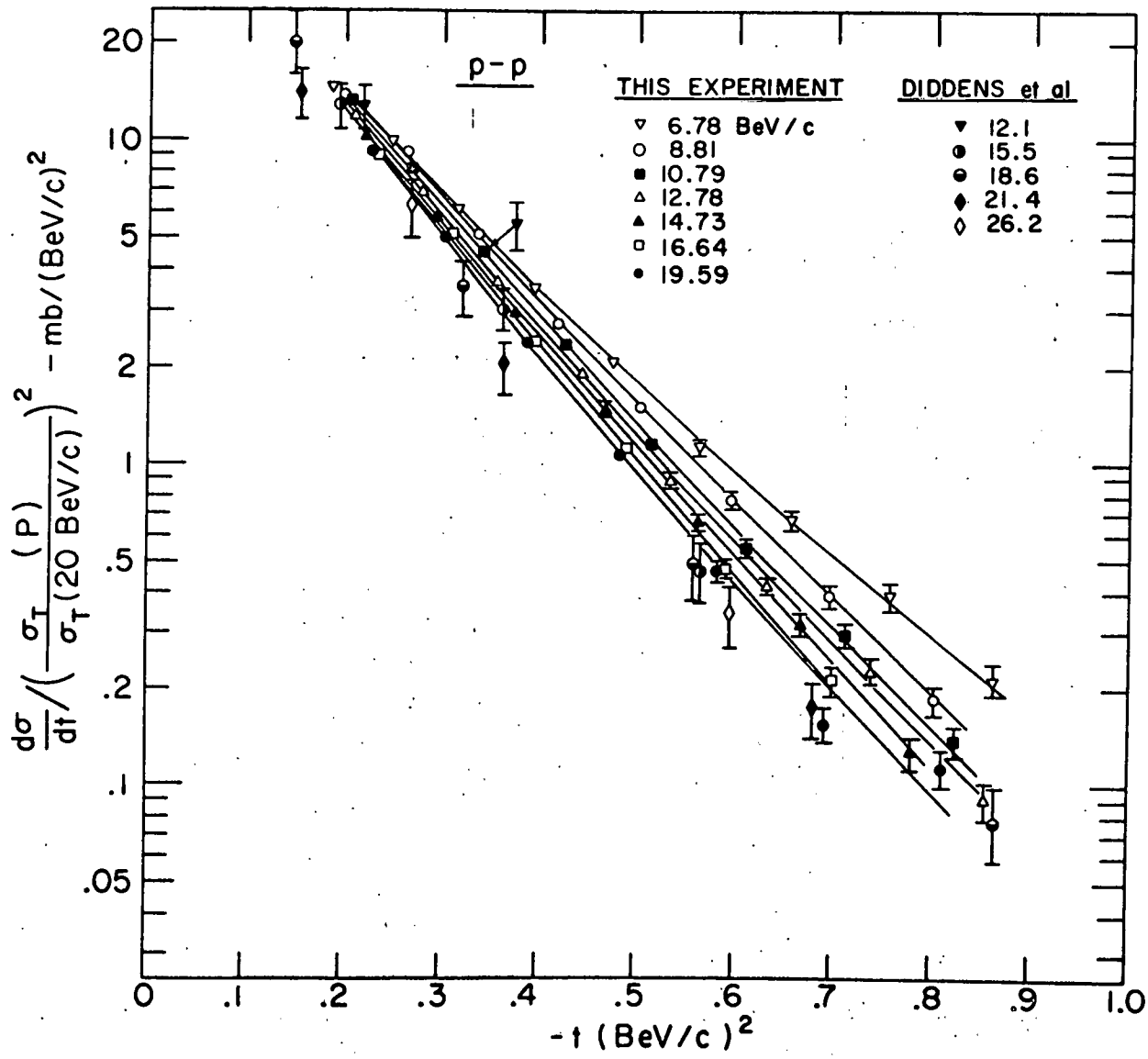
p-p
THIS EXPERIMENT
6.78 BeV/c
8.81
10.79
12.78
14.73
16.64
19.59
DIDDENS et al
12.1
15.5
18.6
21.4
26.2
$\frac{d\sigma}{dt}/\left(\frac{\sigma_T(P)}{\sigma_T(20\ BeV/c)}\right)^2$ - mb/(BeV/c)^2
-t (BeV/c)^2
20
10
5
2
1
.5
.2
.1
.05
0
.1
.2
.3
.4
.5
.6
.7
.8
.9
1.0

FIGURE 3

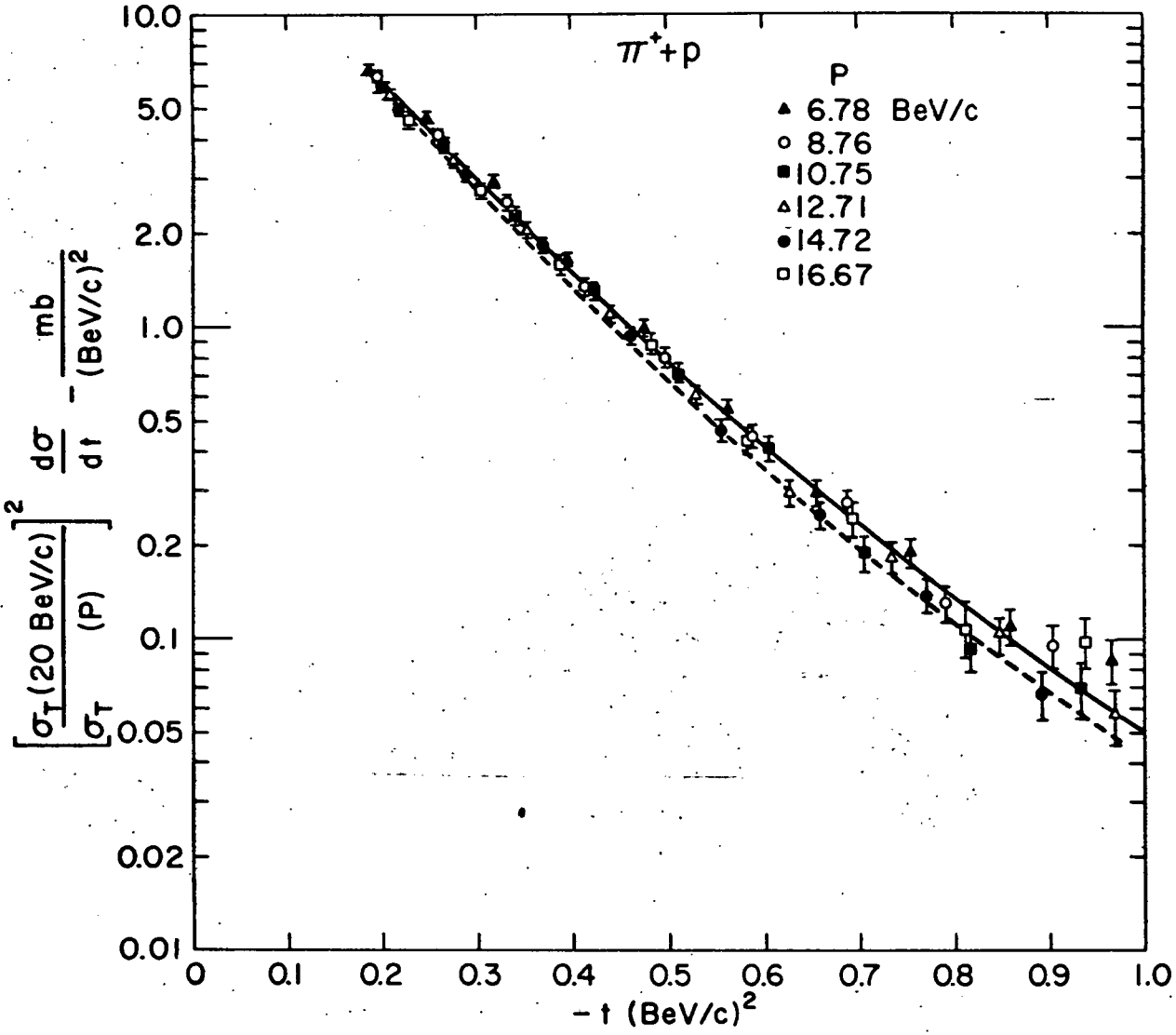
$\pi^+ + p$
P
▲ 6.78 BeV/c
○ 8.76
■ 10.75
△ 12.71
● 14.72
□ 16.67
$\left[\frac{\sigma_T(20\ \text{BeV/c})}{\sigma_T\ (P)}\right]^2 \frac{d\sigma}{dt} - \frac{\text{mb}}{(\text{BeV/c})^2}$
$-t\ (\text{BeV/c})^2$
10.0
5.0
2.0
1.0
0.5
0.2
0.1
0.05
0.02
0.01
0
0.1
0.2
0.3
0.4
0.5
0.6
0.7
0.8
0.9
1.0

FIGURE 4

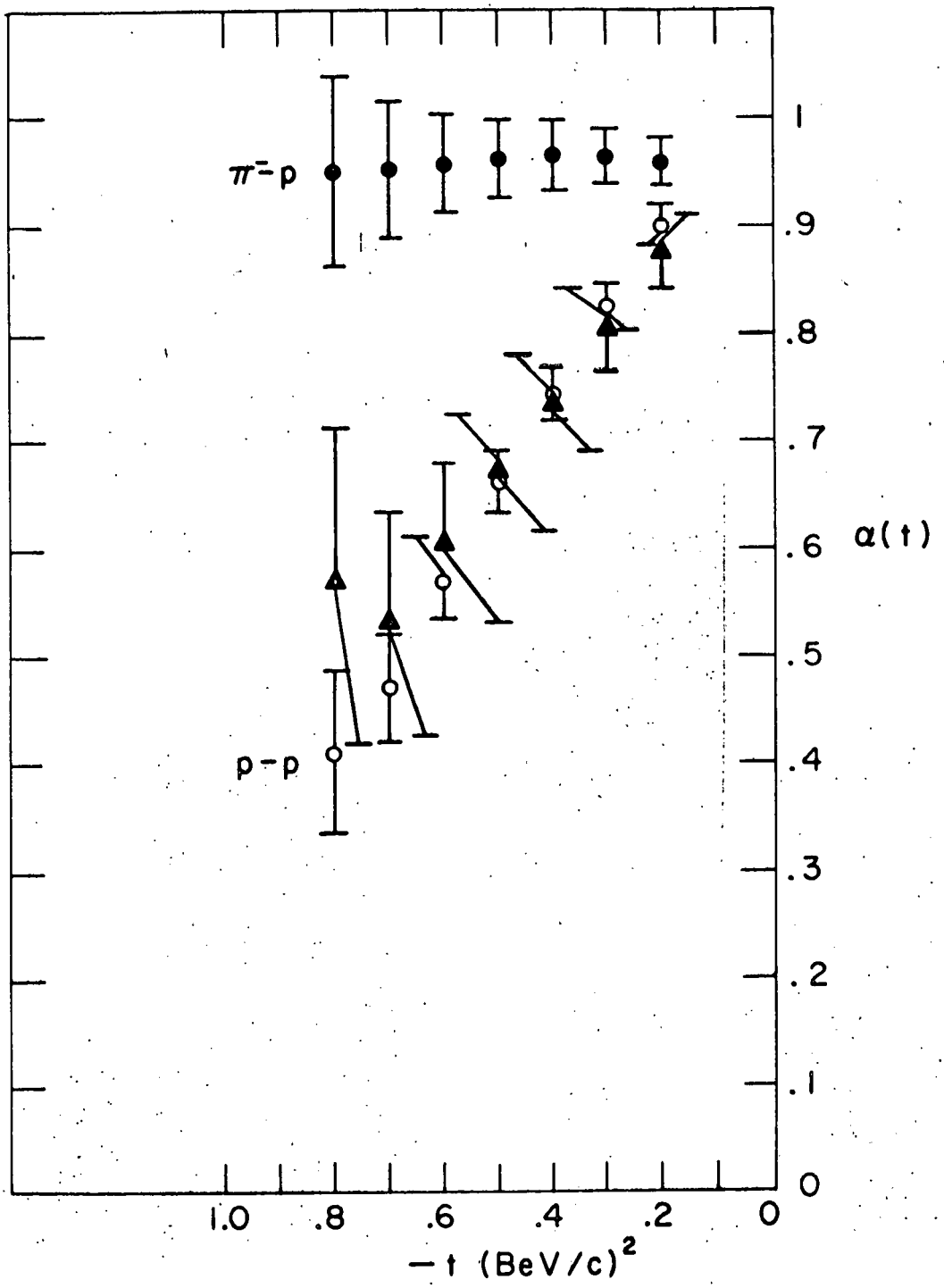

FIGURE 5a.

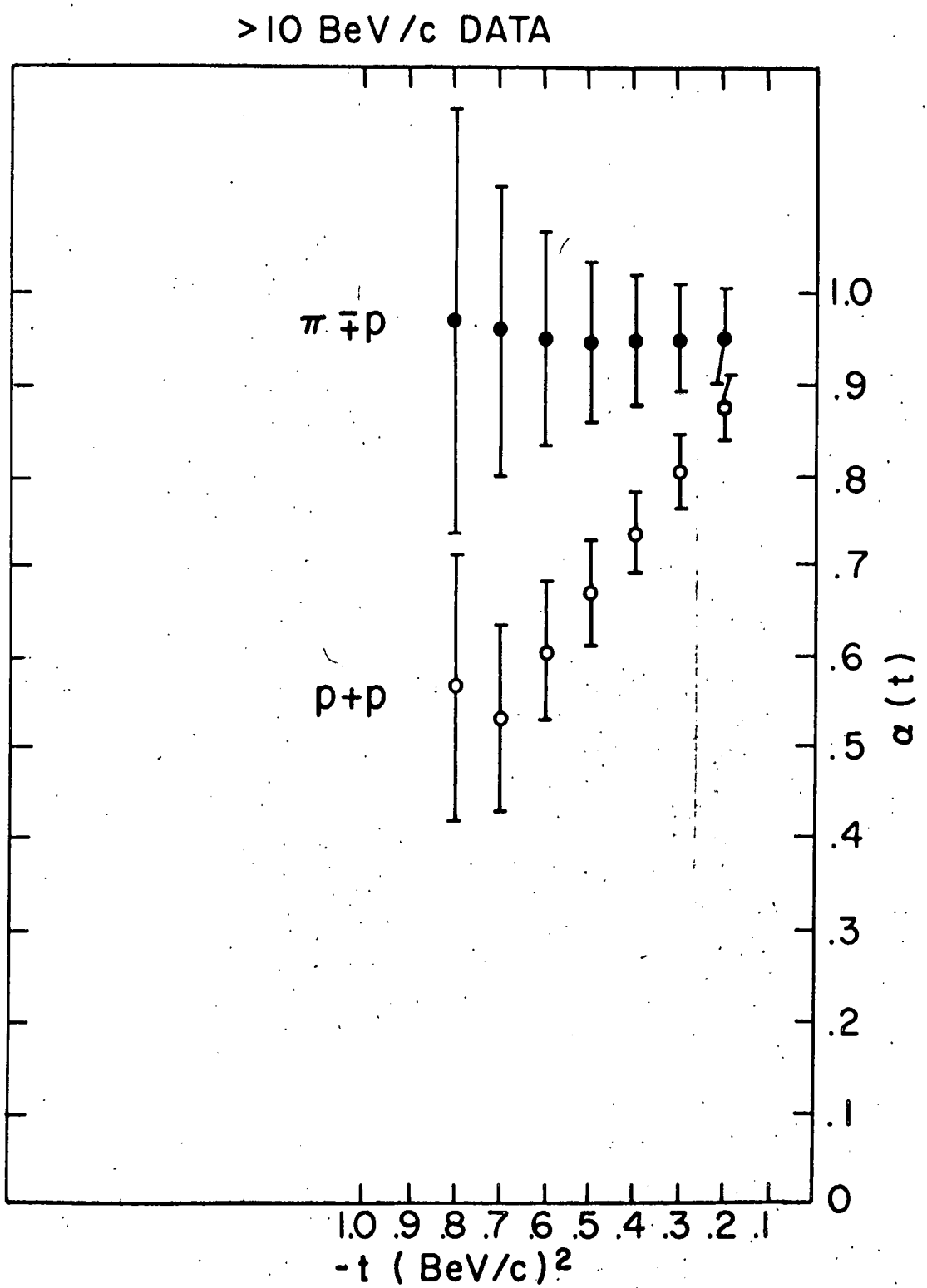

FIGURE 5b.

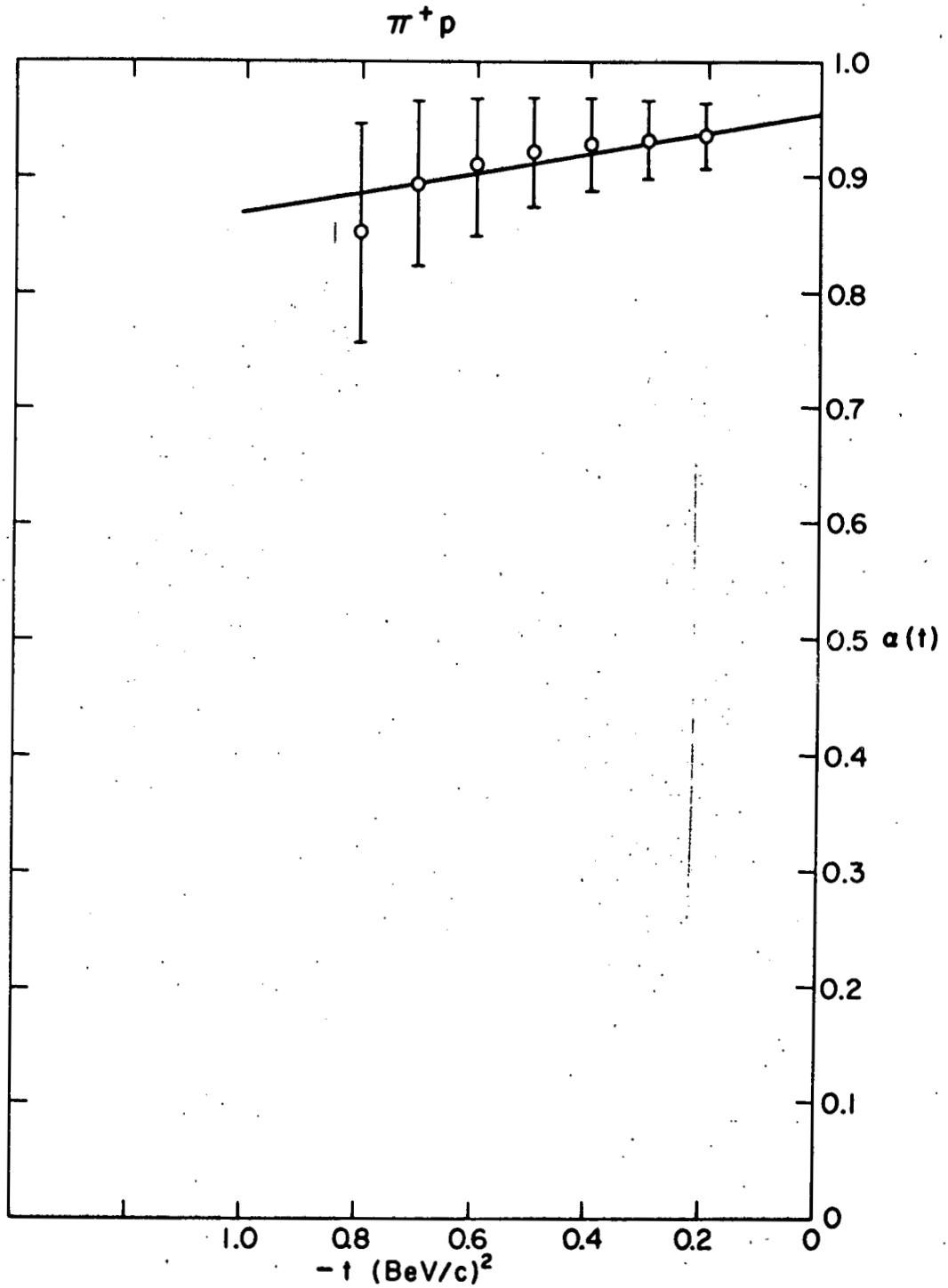

FIGURE 6

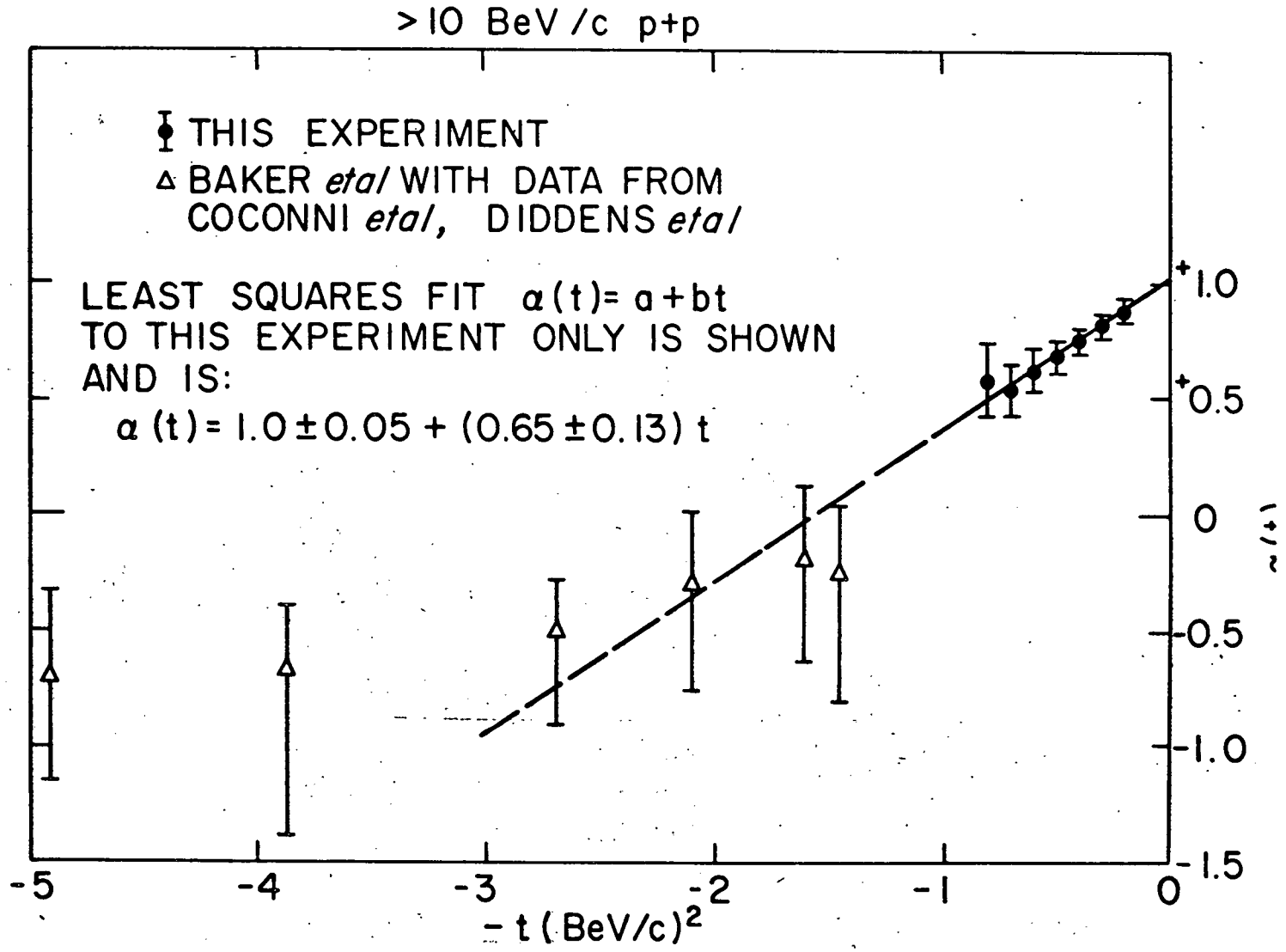
>10 BeV/c p+p
THIS EXPERIMENT
BAKER *etal* WITH DATA FROM
COCONNI *etal*, DIDDENS *etal*
LEAST SQUARES FIT $\alpha(t) = a + bt$
TO THIS EXPERIMENT ONLY IS SHOWN
AND IS:
$\alpha(t) = 1.0 \pm 0.05 + (0.65 \pm 0.13)\, t$
+1.0
+0.5
0
-0.5
-1.0
-1.5
$\alpha(t)$
-5
-4
-3
-2
-1
0
$-t\,(\mathrm{BeV/c})^2$

FIGURE 7

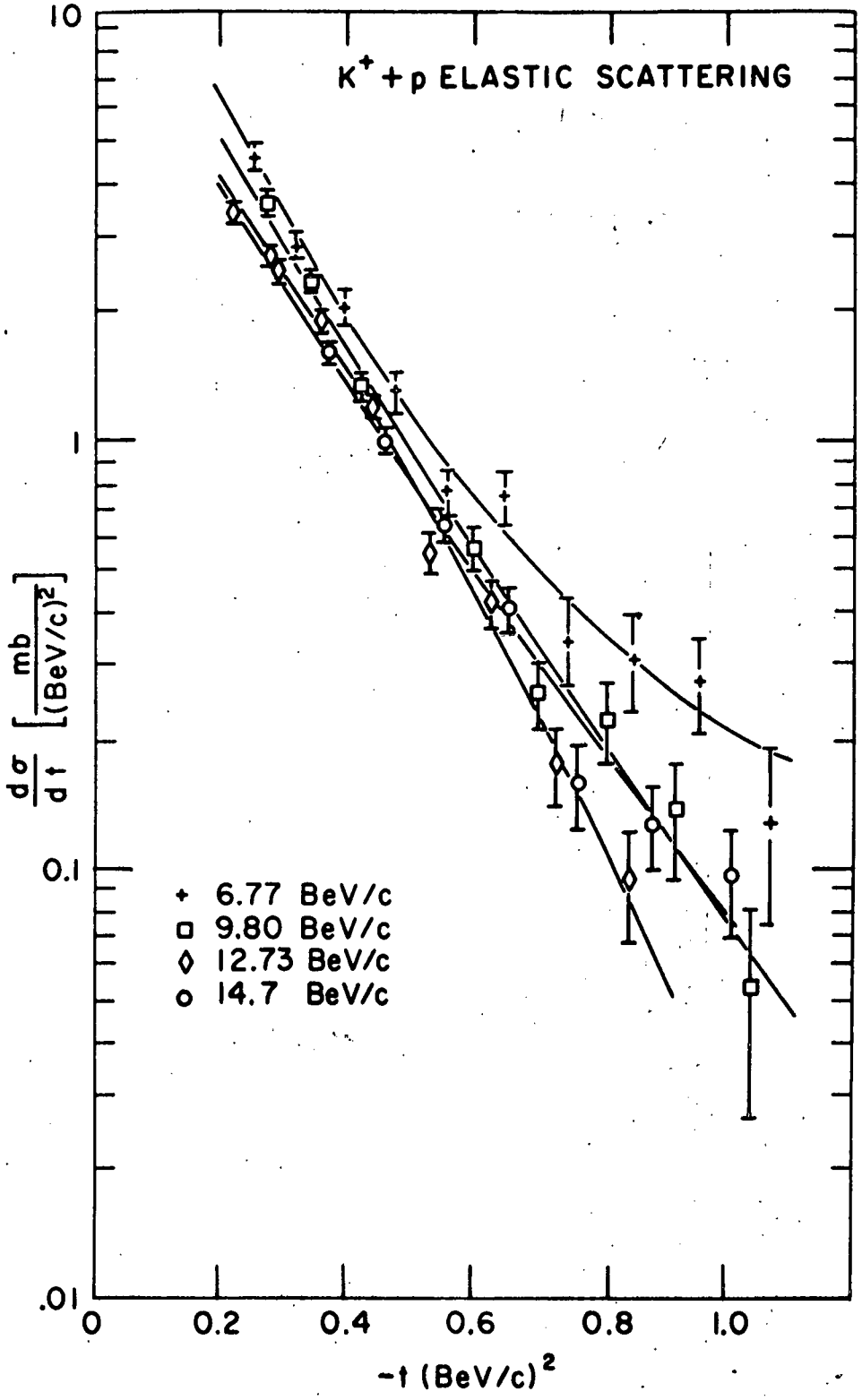
K⁺ + p ELASTIC SCATTERING
10
1
0.1
.01
0
0.2
0.4
0.6
0.8
1.0
dσ/dt [mb/(BeV/c)²]
-t (BeV/c)²
+ 6.77 BeV/c
□ 9.80 BeV/c
◇ 12.73 BeV/c
○ 14.7 BeV/c

FIGURE 8

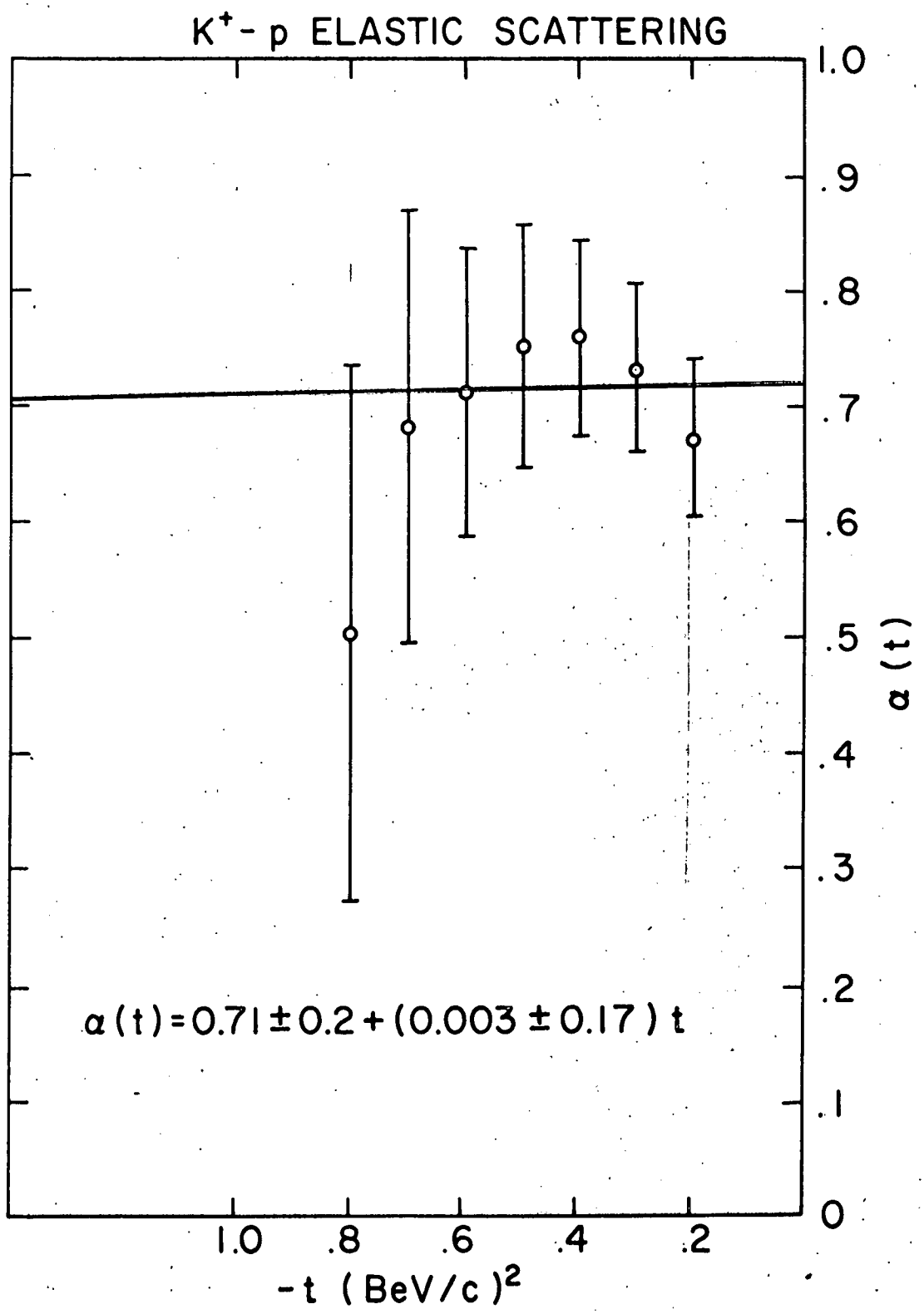
K+ - p ELASTIC SCATTERING
1.0
.9
.8
.7
.6
.5
.4
.3
.2
.1
0
α (t)
α(t) = 0.71 ± 0.2 + (0.003 ± 0.17) t
1.0
.8
.6
.4
.2
-t (BeV/c)²

FIGURE 9

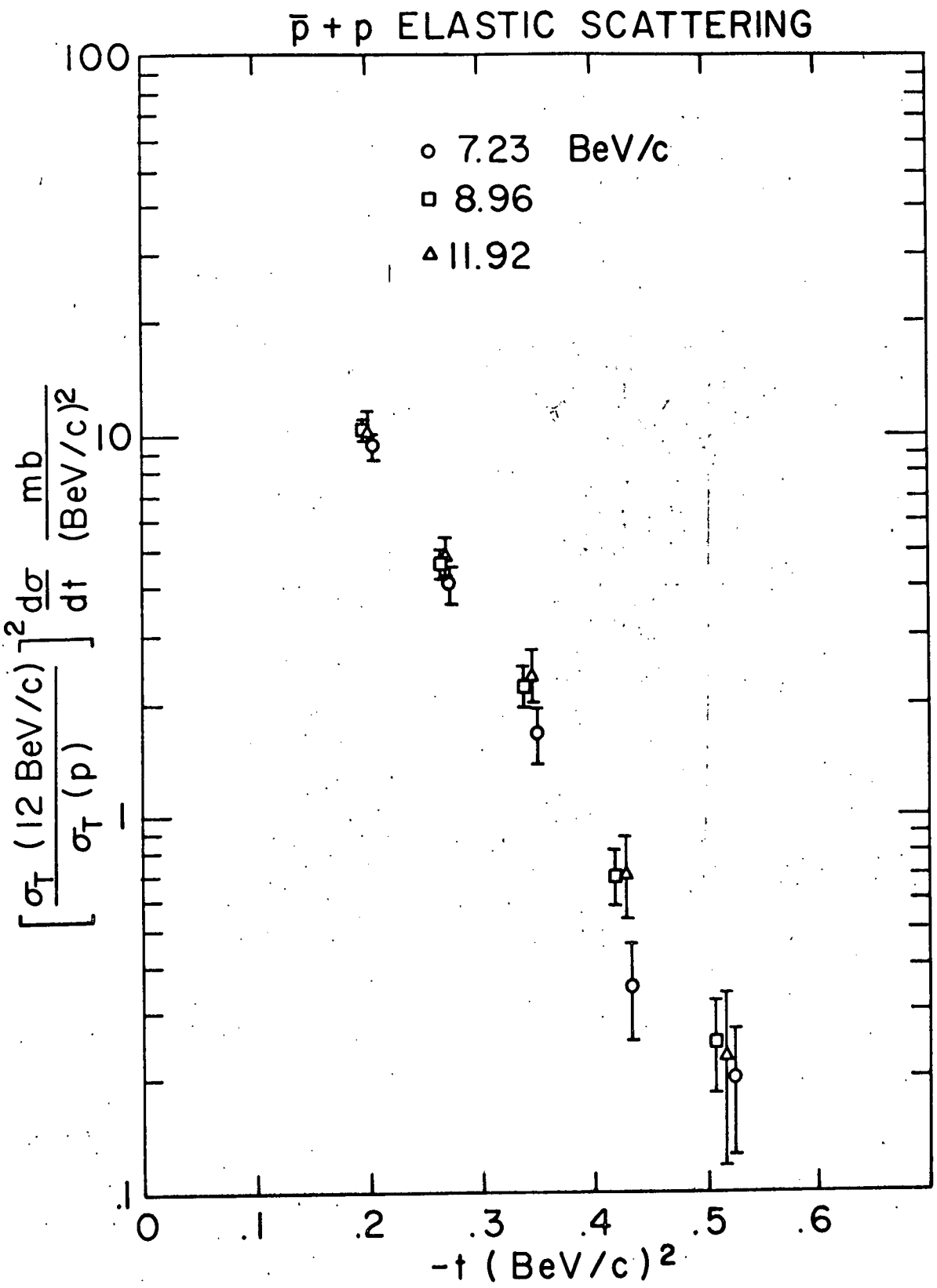
$\bar{p}$ + p ELASTIC SCATTERING
100
10
1
0
.1
.2
.3
.4
.5
.6
○ 7.23 BeV/c
□ 8.96
△ 11.92
$\left[\frac{\sigma_T\ (12\ \text{BeV/c})}{\sigma_T\ (p)}\right]^2 \frac{d\sigma}{dt}\ \frac{\text{mb}}{(\text{BeV/c})^2}$
$-t\ (\text{BeV/c})^2$

FIGURE 10

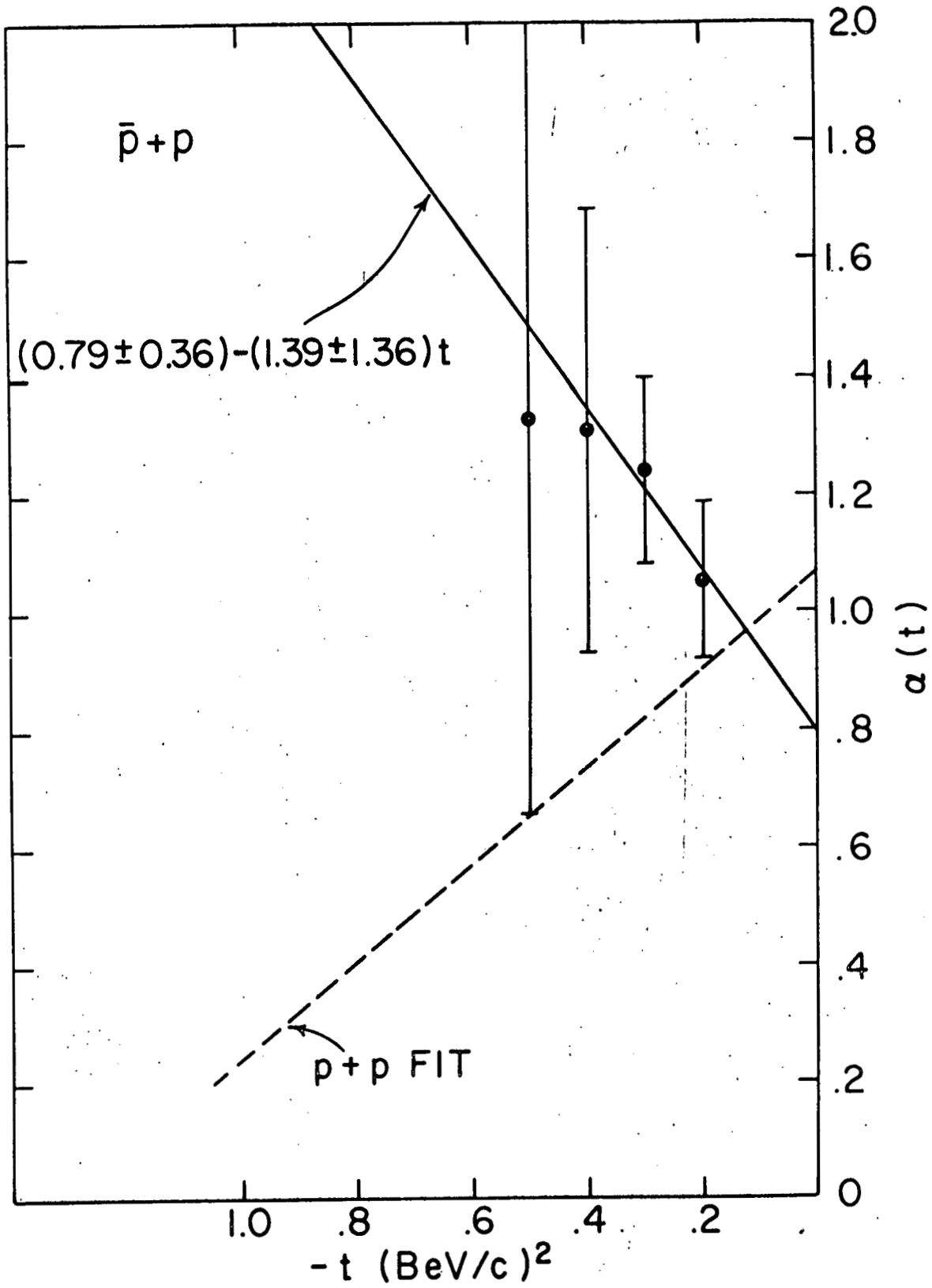
$\bar{p}+p$
$(0.79\pm0.36)-(1.39\pm1.36)t$
$p+p$ FIT
2.0
1.8
1.6
1.4
1.2
1.0
.8
.6
.4
.2
0
$\alpha(t)$
1.0
.8
.6
.4
.2
$-t$ (BeV/c)^2

FIGURE 11

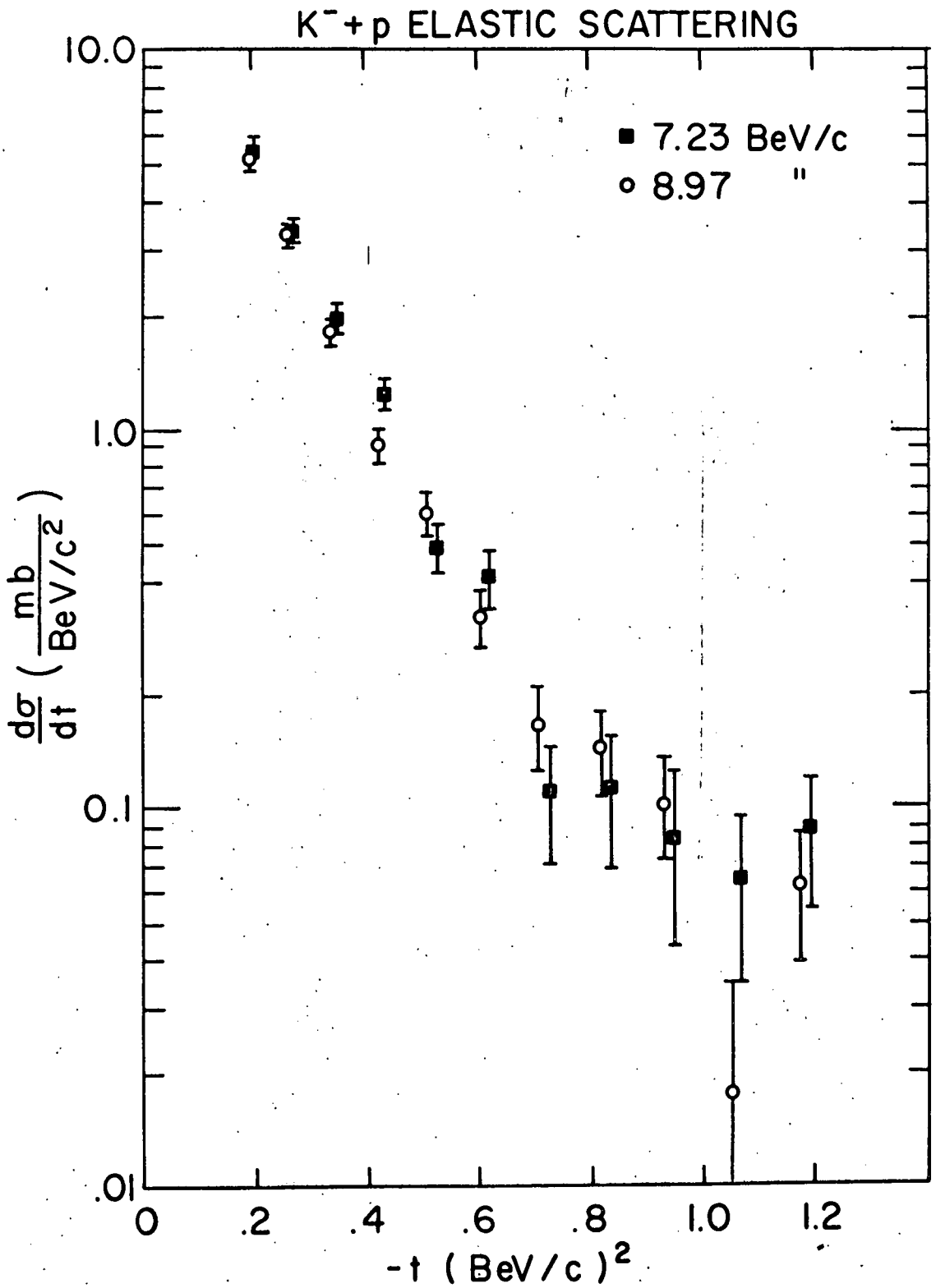
K⁻+p ELASTIC SCATTERING
10.0
1.0
0.1
.01
■ 7.23 BeV/c
○ 8.97 "
dσ/dt (mb/BeV/c²)
0
.2
.4
.6
.8
1.0
1.2
-t (BeV/c)²

FIGURE 12

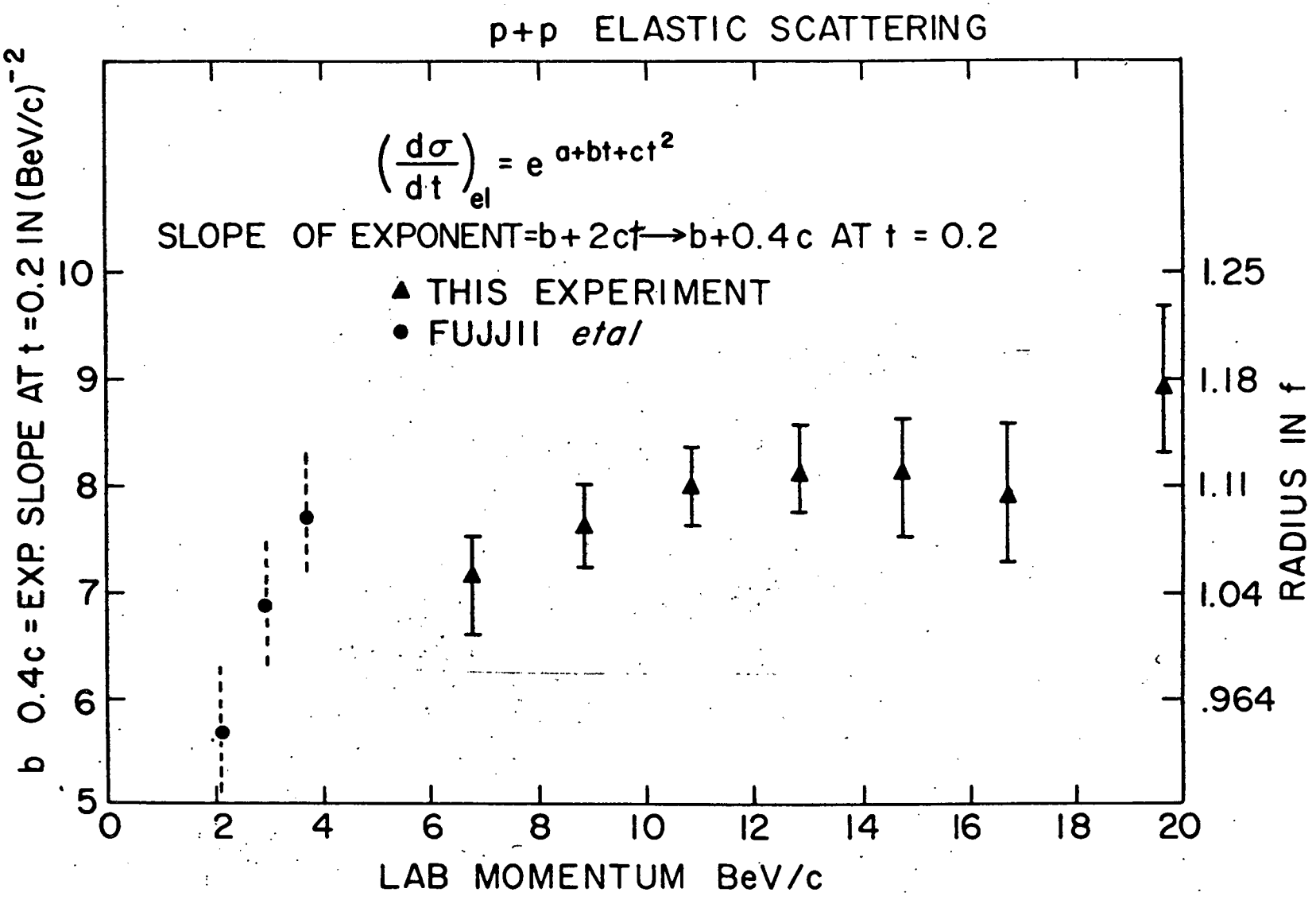
p+p ELASTIC SCATTERING
$\left(\frac{d\sigma}{dt}\right)_{el} = e^{a+bt+ct^2}$
SLOPE OF EXPONENT=b+2ct⟶b+0.4c AT t = 0.2
▲ THIS EXPERIMENT
● FUJJII *etal*
b 0.4c = EXP. SLOPE AT t=0.2 IN (BeV/c)$^{-2}$
RADIUS IN f
1.25
1.18
1.11
1.04
.964
10
9
8
7
6
5
0
2
4
6
8
10
12
14
16
18
20
LAB MOMENTUM BeV/c

FIGURE 13

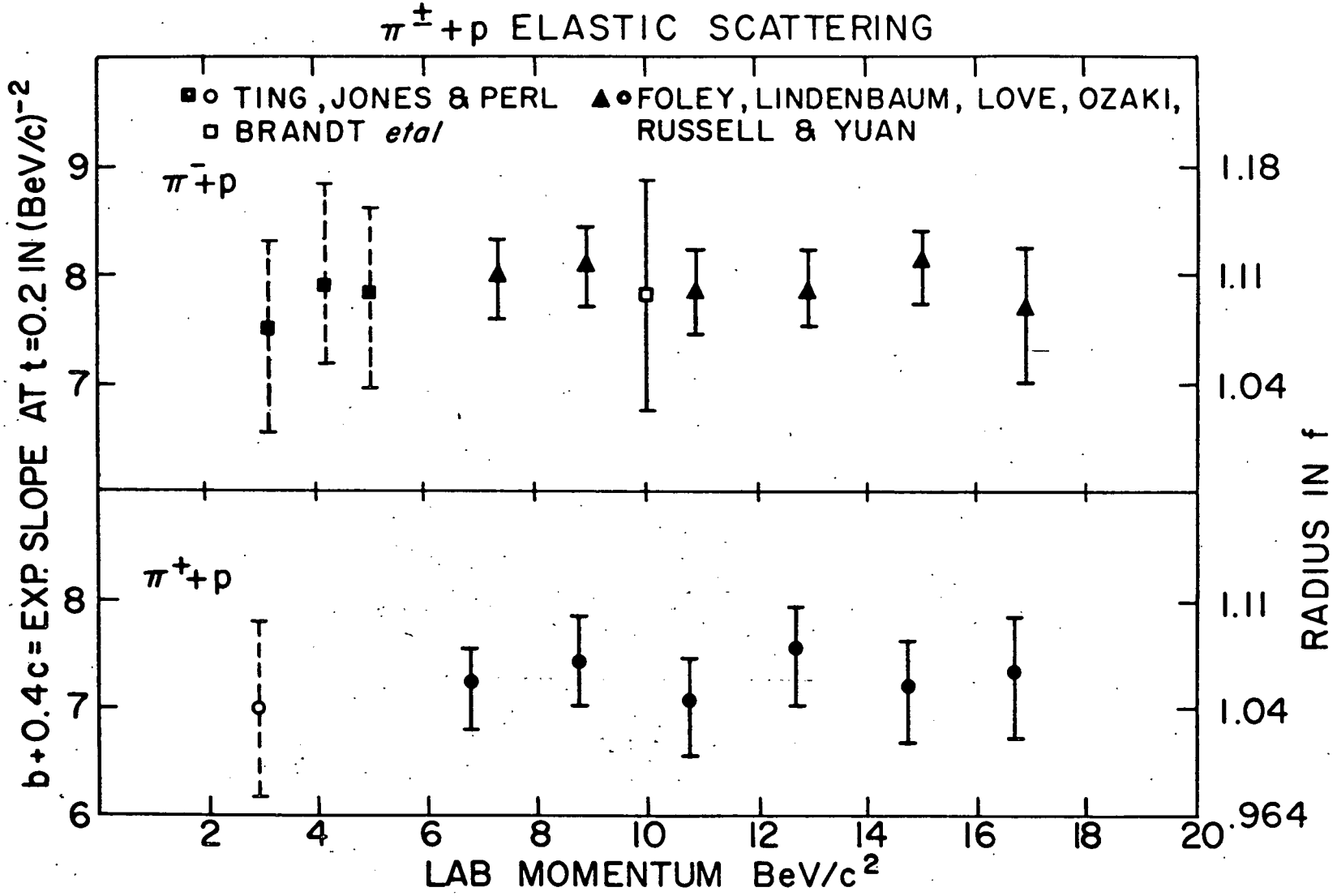
$\pi^{\pm}$+p ELASTIC SCATTERING
TING, JONES & PERL
BRANDT *etal*
FOLEY, LINDENBAUM, LOVE, OZAKI, RUSSELL & YUAN
π^-+p
π^++p
b+0.4c = EXP. SLOPE AT t=0.2 IN (BeV/c)$^{-2}$
RADIUS IN f
LAB MOMENTUM BeV/c^2
9
8
7
6
2
4
6
8
10
12
14
16
18
20
1.18
1.11
1.04
1.11
1.04
.964

FIGURE 14

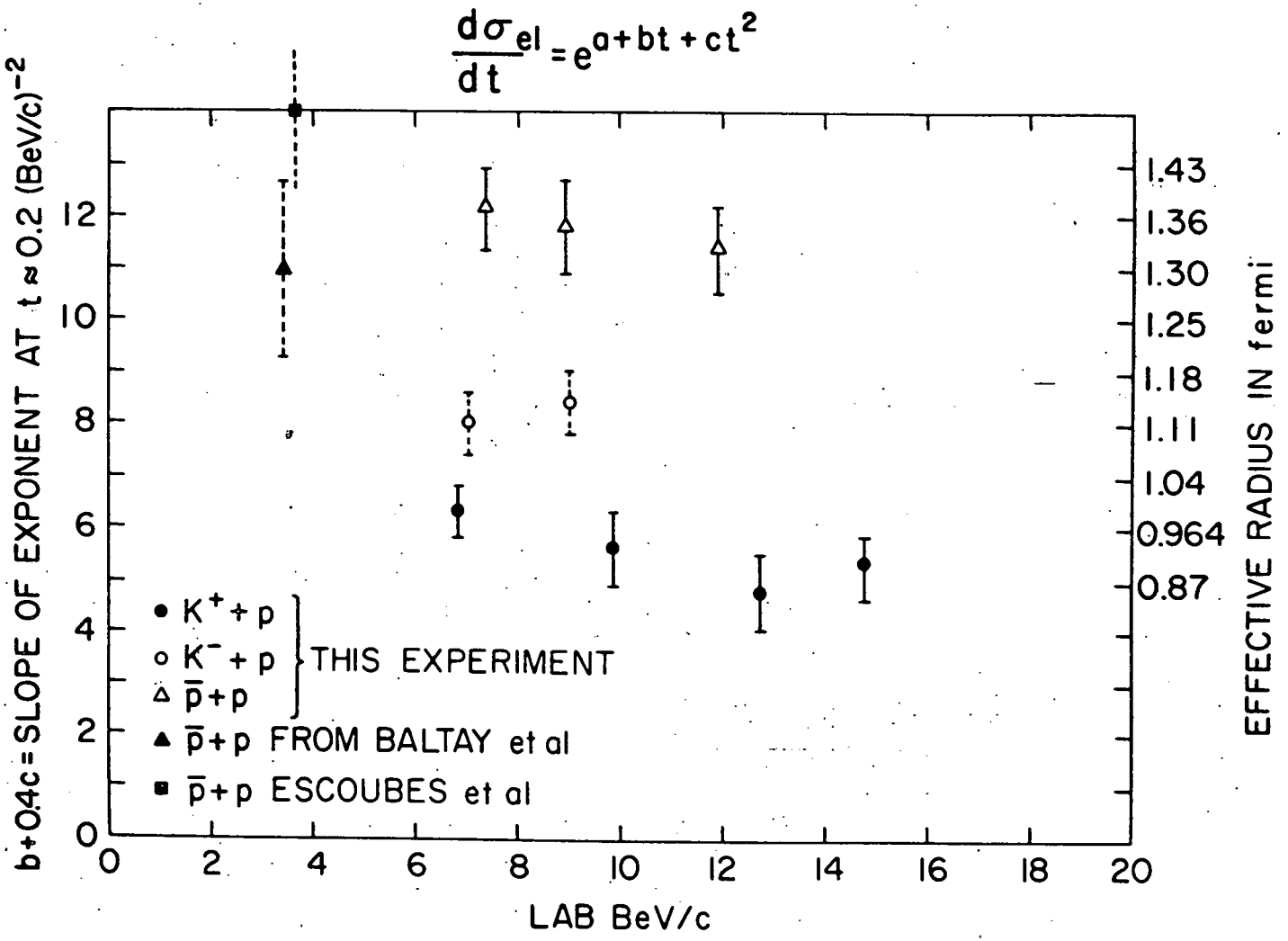
$\frac{d\sigma_{el}}{dt} = e^{a+bt+ct^2}$
b+0.4c = SLOPE OF EXPONENT AT t ≈ 0.2 (BeV/c)$^{-2}$
EFFECTIVE RADIUS IN fermi
LAB BeV/c
0
2
4
6
8
10
12
14
16
18
20
1.43
1.36
1.30
1.25
1.18
1.11
1.04
0.964
0.87
$K^+ + p$
$K^- + p$
$\bar{p}+p$
THIS EXPERIMENT
$\bar{p}+p$ FROM BALTAY et al
$\bar{p}+p$ ESCOUBES et al

FIGURE 15

SCHEMATIC OF HODOSCOPE SYSTEM FOR BROOKHAVEN AGS ELASTIC SCATTERING EXPERIMENTS (SET-UP I)

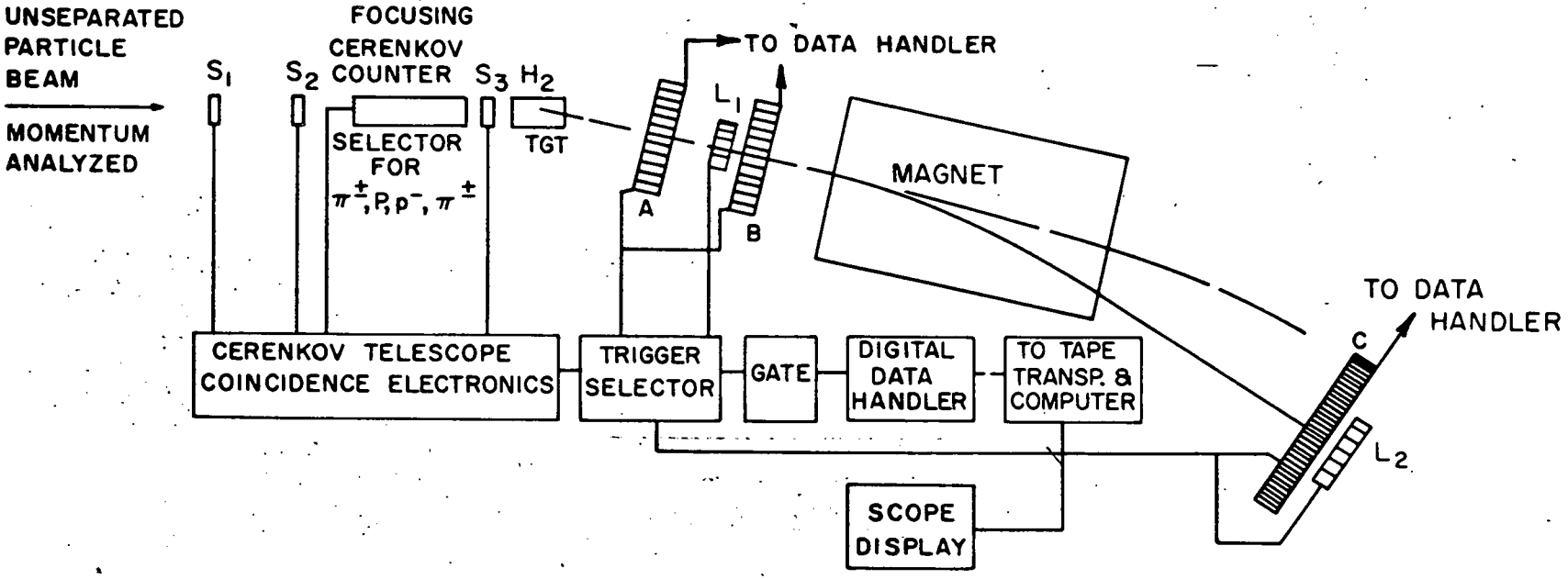

FIGURE 16

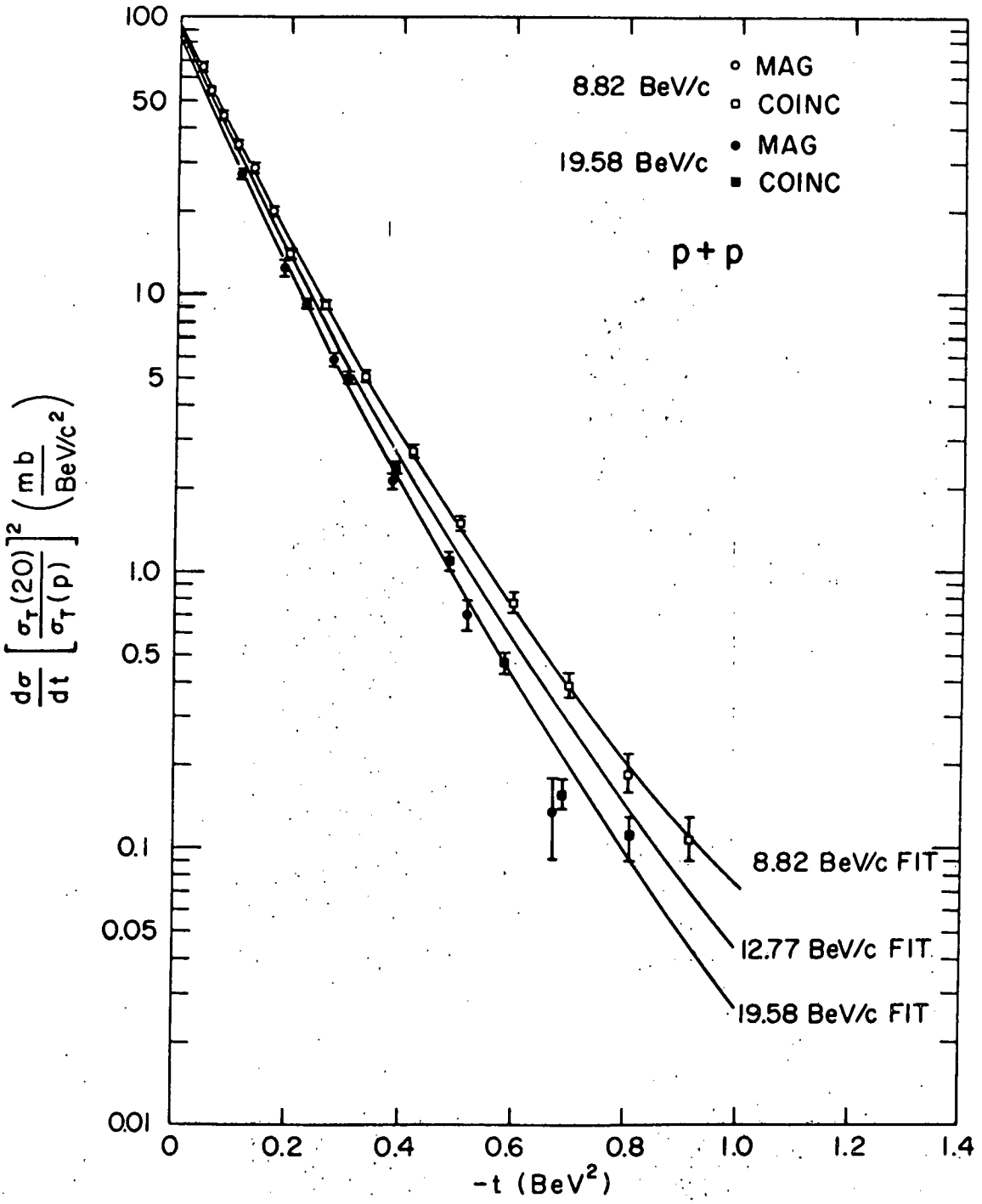
100
50
10
5
1.0
0.5
0.1
0.05
0.01
0
0.2
0.4
0.6
0.8
1.0
1.2
1.4
$\frac{d\sigma}{dt}\left[\frac{\sigma_T(20)}{\sigma_T(p)}\right]^2\left(\frac{mb}{BeV/c^2}\right)$
$-t\ (BeV^2)$
8.82 BeV/c
MAG
COINC
19.58 BeV/c
MAG
COINC
p + p
8.82 BeV/c FIT
12.77 BeV/c FIT
19.58 BeV/c FIT

FIGURE 17

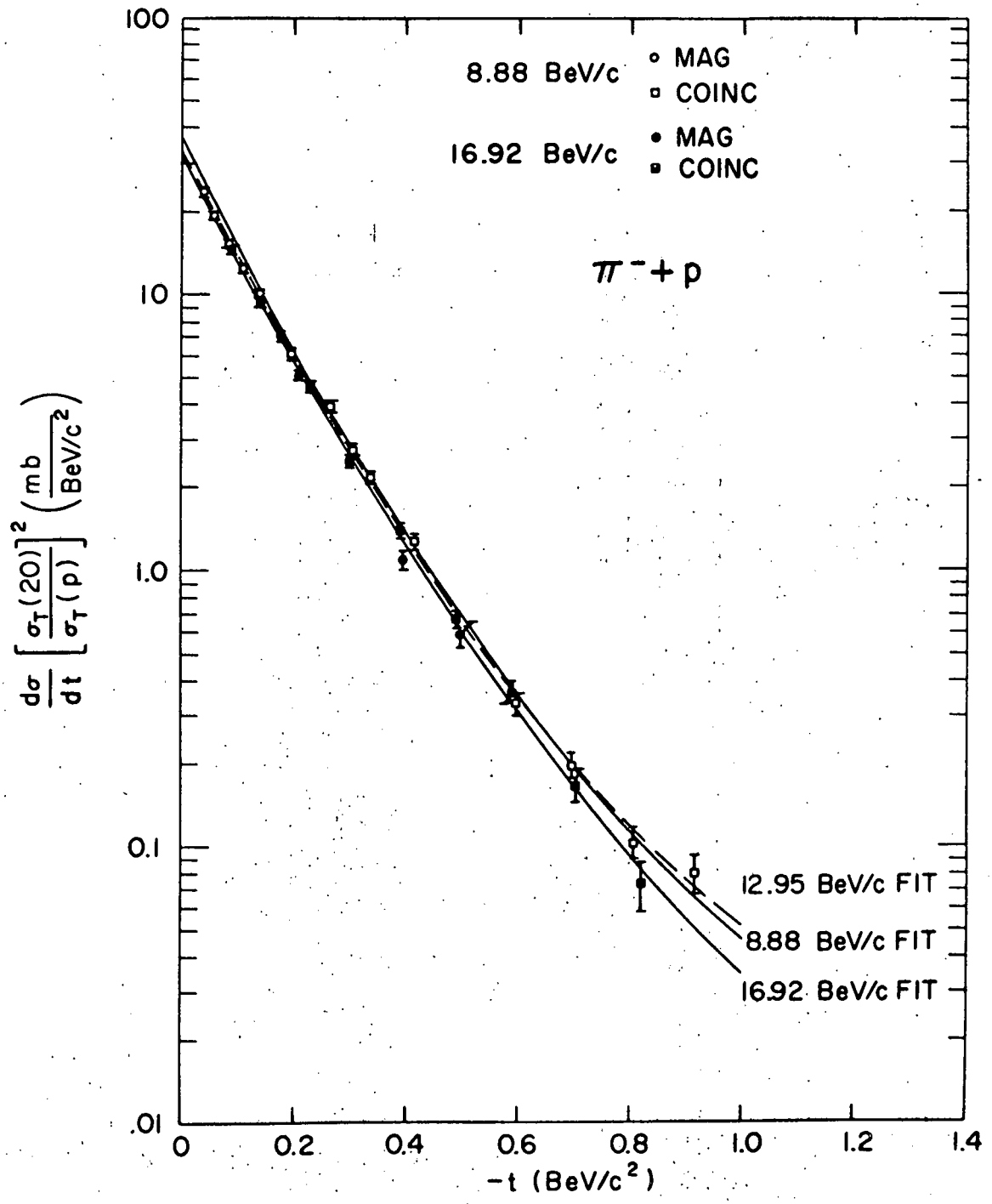
100
10
1.0
0.1
.01
0
0.2
0.4
0.6
0.8
1.0
1.2
1.4
8.88 BeV/c
MAG
COINC
16.92 BeV/c
MAG
COINC
$\pi^- + p$
12.95 BeV/c FIT
8.88 BeV/c FIT
16.92 BeV/c FIT
$\frac{d\sigma}{dt}\left[\frac{\sigma_T(20)}{\sigma_T(p)}\right]^2 \left(\frac{mb}{BeV/c^2}\right)$
$-t\ (BeV/c^2)$

FIGURE 18

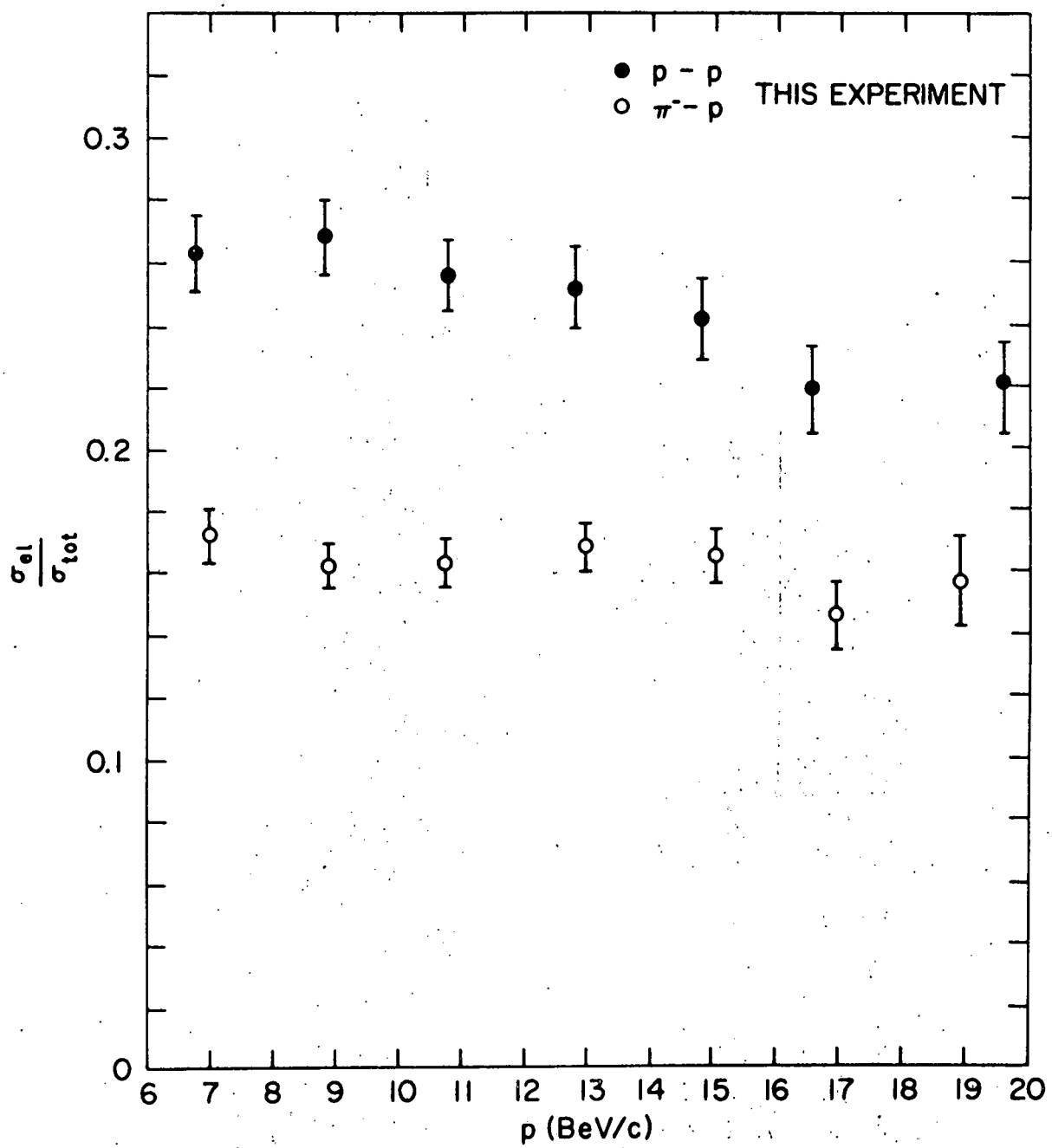
p - p
π⁻ - p
THIS EXPERIMENT
0.3
0.2
0.1
0
σel / σtot
6
7
8
9
10
11
12
13
14
15
16
17
18
19
20
p (BeV/c)

FIGURE 19

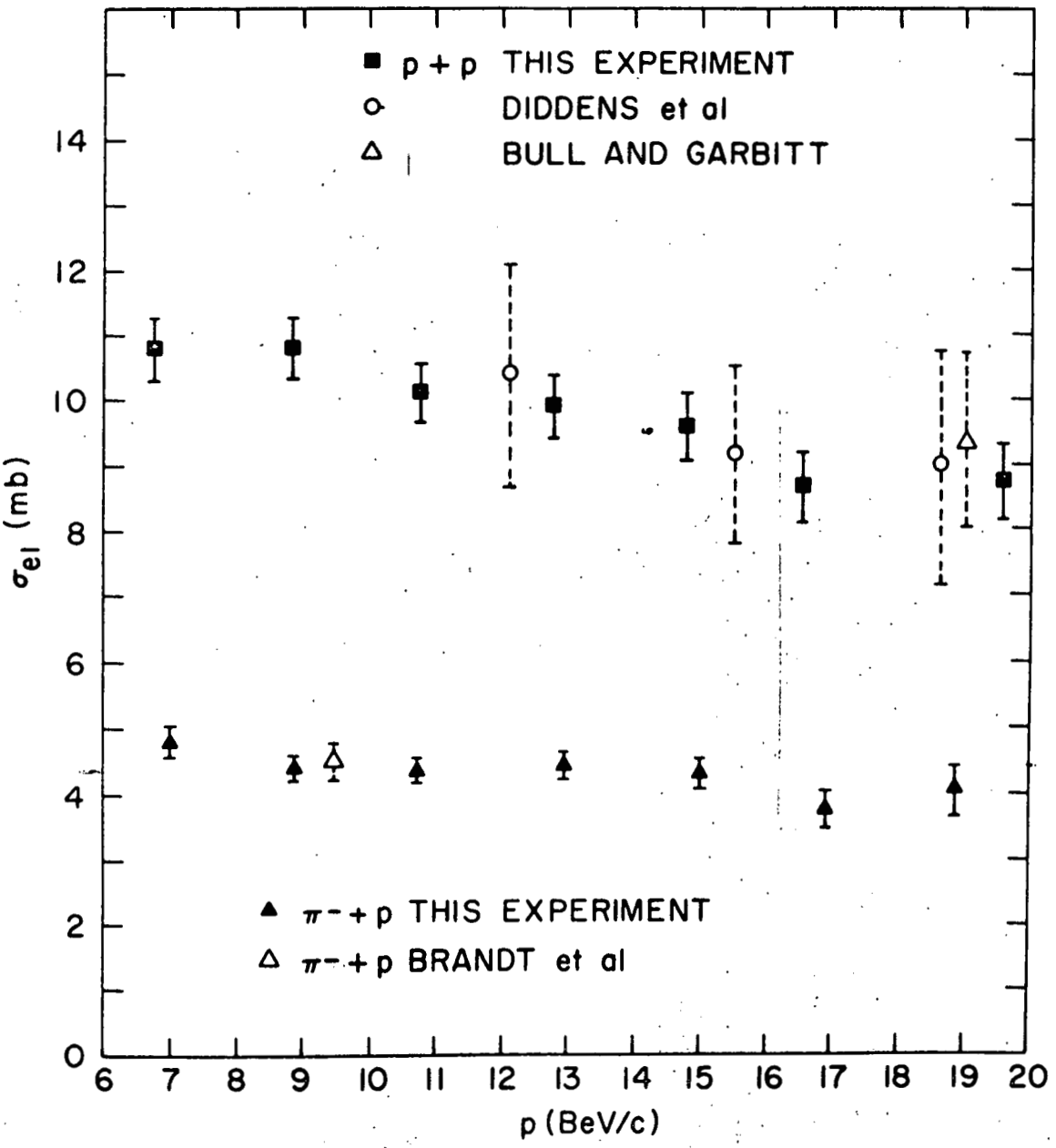
p + p THIS EXPERIMENT
DIDDENS et al
BULL AND GARBITT
π⁻ + p THIS EXPERIMENT
π⁻ + p BRANDT et al
σel (mb)
p (BeV/c)
0
2
4
6
8
10
12
14
6
7
8
9
10
11
12
13
14
15
16
17
18
19
20

FIGURE 20 a.

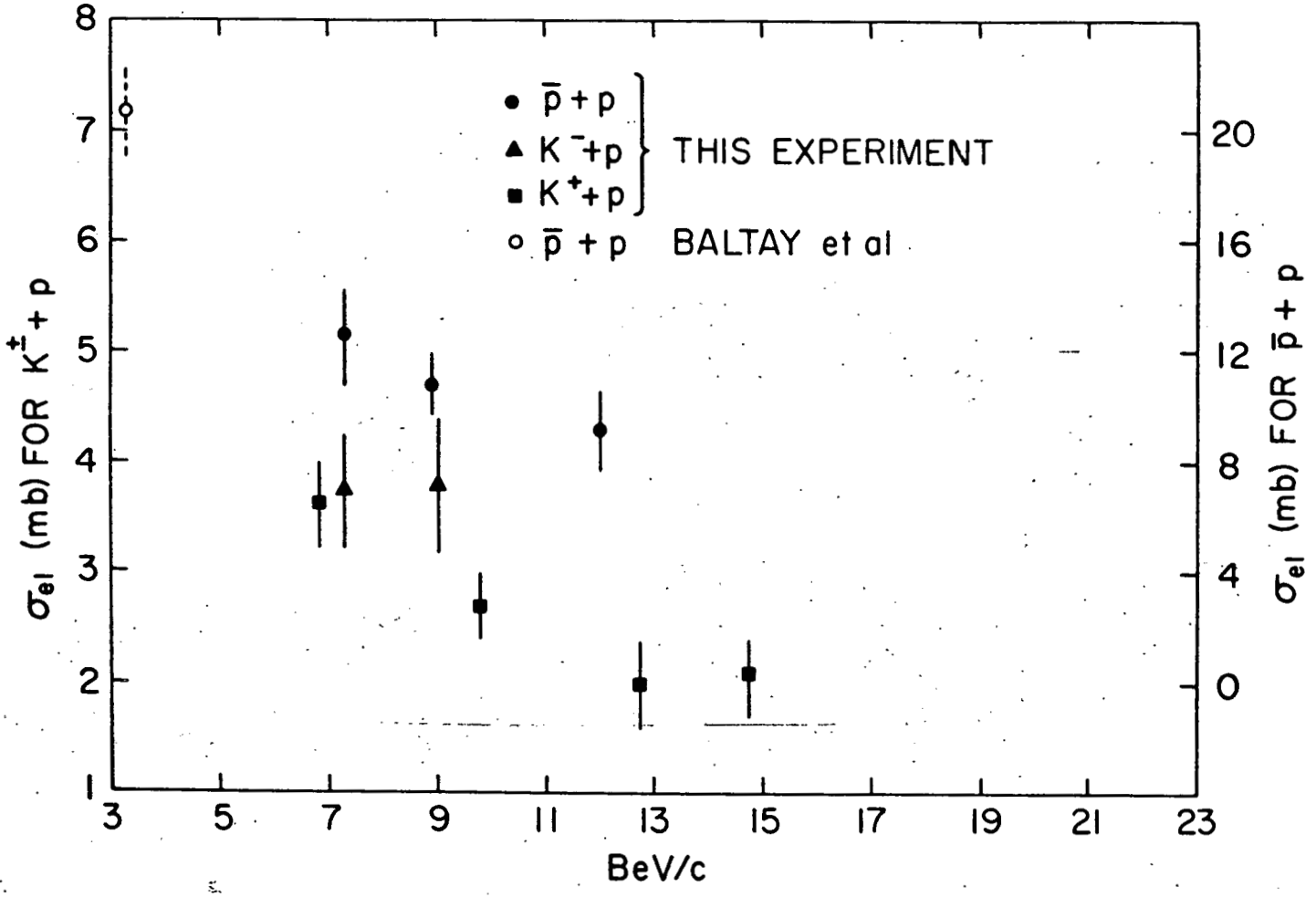
● $\bar{p}+p$
▲ K^-+p
■ K^++p
THIS EXPERIMENT
○ $\bar{p}+p$ BALTAY et al
σ_{el} (mb) FOR $K^{\pm}+p$
σ_{el} (mb) FOR $\bar{p}+p$
BeV/c
8
7
6
5
4
3
2
1
20
16
12
8
4
0
3
5
7
9
11
13
15
17
19
21
23

FIGURE 20 b

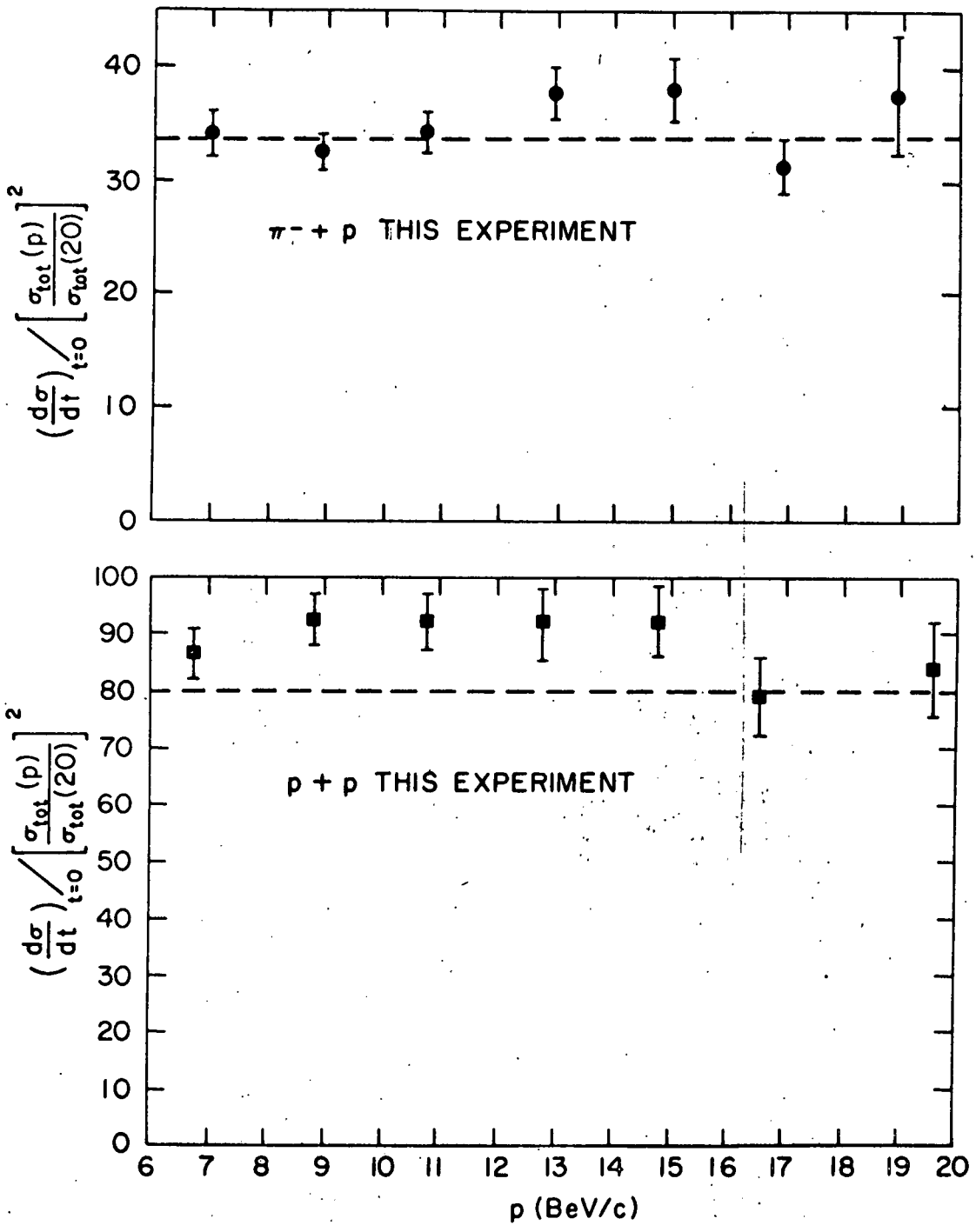
$\left(\frac{d\sigma}{dt}\right)_{t=0} \Big/ \left[\frac{\sigma_{tot}(p)}{\sigma_{tot}(20)}\right]^2$
$\pi^- + p$ THIS EXPERIMENT
$p + p$ THIS EXPERIMENT
0
10
20
30
40
50
60
70
80
90
100
6
7
8
9
10
11
12
13
14
15
16
17
18
19
20
p (BeV/c)

FIGURE 21